

**KERNFORSCHUNGSZENTRUM  
KARLSRUHE**

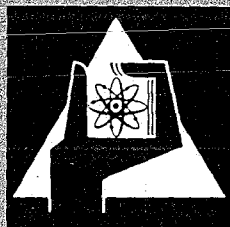
Januar 1972

KFK 1372

Institut für Experimentelle Kernphysik

**A. C. Losses in Superconducting Pulsed Magnets**

G. Ries, H. Brechna



GESELLSCHAFT FÜR KERNFORSCHUNG M. B. H.

KARLSRUHE



KERNFORSCHUNGSZENTRUM KARLSRUHE

January 1972

KFK 1372

Institut für Experimentelle Kernphysik

A.C. Losses in Superconducting Pulsed Magnets.

G. Ries, H. Brechna

Gesellschaft für Kernforschung m.b.H., Karlsruhe



## Zusammenfassung

Die Theorie der Wechselstromverluste von gepulsten Typ II Supraleiter und supraleitender Magnete ist präsentiert. Die berechneten Verluste in Magneten sind mit gemessenen Werten verglichen. Verschiedene Verlustmessmethoden sind beschrieben.

## Abstract:

The theory and calculation of a.c. losses in type II superconducting materials and superconducting coils are presented. The calculated losses are compared to loss-measurements in solenoids performed by several laboratories. Methods of loss measurements are described.

## C o n t e n t s:

1.	A.C. losses in superconducting pulsed magnets	1
1.1	Introduction	1
1.2	Flux profiles	6
1.3	Thin superconductors	7
1.4	Finite size slabs and cylindrical conductors	8
1.5	Methods of calculating hysteretic losses	8
1.6	Hysteretic losses in slabs	9
1.7	Application to multifilament conductors	14
1.8	Hysteretic losses in cylindrical shaped superconductors	17
1.9	Hysteretic losses in coils using hollow superconducting filaments	20
1.10	Losses in composites	21
1.11	Eddy current losses in the conductor matrix	21
1.12	Self field losses	29
1.13	Contribution of external fields	33
1.14	Discussion	
1.15	Comparison between self field and hysteretic losses	35
1.16	Modification of hysteretic losses, if the transport current is zero	36
2.	Additional effects in twisted multifilament conductors	37
2.1	Axial diffusion of the self field	37
2.2	Extension of the self field model in twisted multifilament conductors	43
3.	Eddy current losses in metallic parts	46
3.1	Iron losses in the flux return path	46
4.	Comparison of loss calculation with experiments	46
5.	Methods of loss measurements	51
5.1	Calorimetric method	51
5.2	Electric methods	51
6.	Figure captions	55
7.	References	57

# 1. A.C. Losses in superconducting pulsed magnets

## 1.1 Introduction

Alternating current losses have been subject to investigation in the past few years, since the development of new multi-filament conductors became reality and the possibility of using them in pulsed synchrotron-magnets became feasible.

In solenoids field changes in the order of 7 T/s have been achieved. In pulsed synchrotron magnets which have more complicated coil geometries field changes of about 6 T/s have been obtained without generating excessive dissipative losses. Depending on the field amplitude superconducting magnets can be pulsed at frequencies  $\leq 1$ Hz. One of the main reasons of these low duty cycle operations are a.c. losses generated in the superconductor and the normal metal substrate, which produces local heating and may lead to degradation of the superconducting material.

Differing from the ideal type II superconductor the inhomogeneities in a nonideal superconductor (dislocations, precipitations, grain boundaries) lead to a spatial variation of the free energy of a vortex  $\mathcal{F}(\vec{r})$  which is shown in Fig. (1.1). In  $\mathcal{F}(\vec{r})$ , the interaction with the neighbouring fluxoids, as well as the line tension of a curved fluxline, is to be included. A Lorentz force  $f_L$  can be regarded as an additional contribution to the free energy

$$\mathcal{F}'(\vec{r}) = \mathcal{F}(\vec{r}) + \vec{f}_L \cdot \vec{r} \quad (1.1)$$

or:

$$\mathcal{F}'(\vec{r}) = \mathcal{F}(\vec{r}) + (\vec{J}_T \times \vec{\phi}_0) \cdot \vec{r} \quad (1.2)$$

with  $\vec{\phi}_0$  the fluxquantum in the direction of the vortex.

The fluxoids are trapped in the potential minima of  $\mathcal{F}'$  and remain stationary until  $\vec{f}_L$  exceeds the maximum pinning force  $\vec{f}_p = \max(\nabla\mathcal{F}(\vec{r}))$  and a minimum in  $\mathcal{F}'$  does not exist further: Dissipative fluxflow occurs at the "critical current"  $J_c$ . The derivation of  $\vec{f}_p$  and thus  $\vec{J}_c$  from the individual fluxoid-defect interaction is extremely complicated by the fact that  $\mathcal{F}(\vec{r})$  is not rigid but dependent on the interfluxoid distance. Thus interaction with the neighbouring fluxoids has to be taken into account. A theoretical approach to get an effective average pinning force  $\langle \vec{f}_p \rangle$  per unit length of fluxoids is given by Labusch<sup>1)</sup>.

The value of  $\vec{J}_c$  with  $\langle \vec{f}_p \rangle = \vec{J}_c \times \vec{\phi}_0$  can not be exactly determined, as due to thermal activation a number of fluxoids can move out of the potential minima at smaller currents than  $\vec{J}_c$ . This leads to a (strongly current and temperature dependent) "flux creep"-voltage<sup>2)</sup> expressed by

$$U \sim \exp(cI/kT). \quad (1.3)$$

Usually  $J_c$  is related to a fixed fluxflow resistivity eg.

$$\rho_F = 10^{-12} \text{ Ohm.cm.}$$

Up to now the external force per vortex unit length was expressed by  $\vec{f}_L = \vec{J}_T \times \vec{\phi}_0$ . This assumption leads to a total force on a conductor of volume  $V$ ,

$$\vec{F}_L = \int_V [\vec{B}(\vec{r}) \times \vec{J}_T(\vec{r})] d^3r \quad (1.4)$$

where we used  $\vec{B} = n \vec{\phi}_0$  and  $n = \text{Fluxline density}$ . This is obviously not identical with the classical magnetic force on the conductor located in a uniform field  $\mu_0 H_{\text{ext}}$ :

$$\vec{F}_M = \mu_0 H_{\text{ext}} \cdot \int_V [\vec{J}_T(\vec{r})] d^3r = \mu_0 H_{\text{ext}} \cdot \vec{I}_T \cdot L \quad (1.5)$$

with  $\vec{H}_{\text{ext}}$ , the external field.

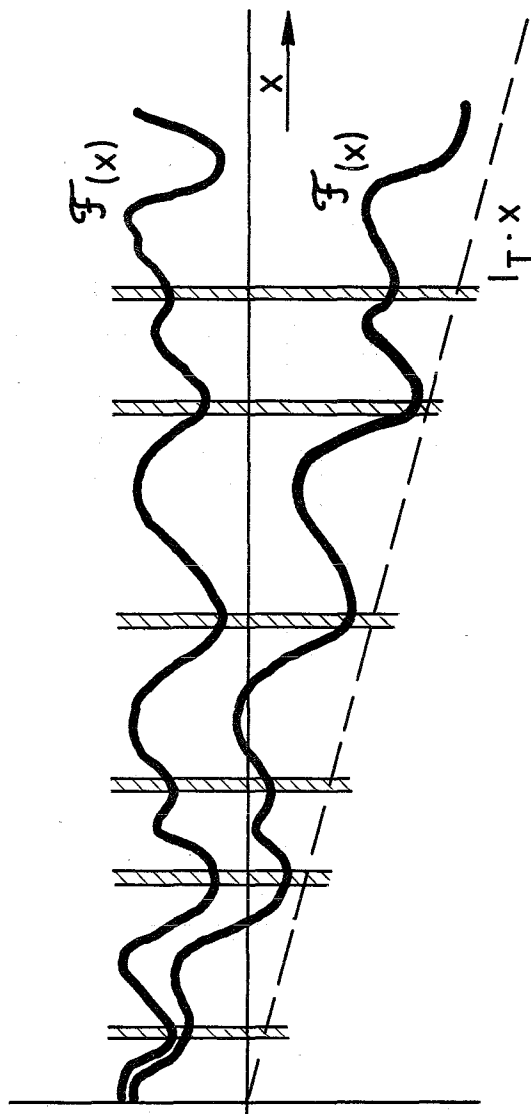


Fig.1.1

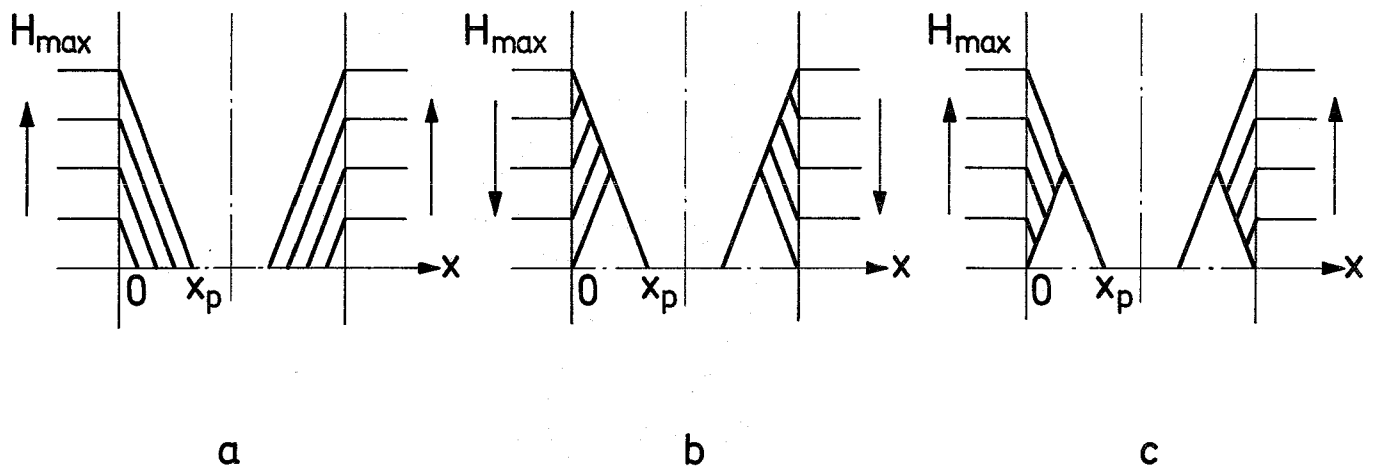


Fig.12

As  $\vec{B}(r)$  in the conductor differs from  $\vec{H}_{\text{ext}}$ , the resulting difference must be attributed to the following additional effects:

The density gradient of flux lines leads to a net force on a fluxoid as the interfluxoid forces do not cancel.

For probes with a demagnetisation factor  $D \neq 0$ , the persistent supercurrents lead to a distortion of the magnetic field inside and outside the superconductor. The curved shape of fluxlines inside the superconductor gives an additional line tension force acting on the pinning centres.

From the free enthalpy  $G(T, H)$ , Friedel, de Gennes and Matricon<sup>3)</sup> have derived an expression for the correction to the force on a fluxline

$$\vec{f}_L = \frac{\partial H(B)}{\partial B} [\vec{J}_T \times \vec{\phi}_0] \quad (1.6)$$

where  $H(B)$  denotes the external field necessary to generate an internal equilibrium induction  $B$  in the ideal (unpinned) superconductor. Eq. (1.6) must fail at least for low fields,  $H \rightarrow H_{c1}$ , where  $\frac{\partial H(B)}{\partial B} \rightarrow 0$ .

In principle the electromagnetic force must result from the Maxwell tensor which is not known, as it presumes detailed knowledge of the internal field.

We suggest to set for the total volume force acting on the fluxline lattice, the relation:

$$\vec{F}_L = \vec{J} \times \mu_0 \vec{H}_{\text{ext}} \quad (1.7)$$

The effective pinning force density  $F_p$  counteracting  $F_L$  is thus

$$n \langle \vec{f}_p \rangle = \vec{F}_p = \mu_0 [\vec{J}_c \times \vec{H}_{\text{ext}}] \quad (1.8)$$

Without the need for a detailed analysis of interfluxoid forces and of the line tension, these effects should automatically be included. The only assumption made here for simplicity is, that the magnetic forces act on the fluxoids alone.

For superconductor geometries regarded here (thin filaments) the condition of  $B \approx H_{\text{ext}}$  is always fulfilled.

Using Maxwells law,  $\text{curl } \vec{H} = \vec{J}$ , the Eq. (1.7) can be written as

$$\vec{F}_L = \mu_0 \cdot [\text{curl } \vec{H} \times \vec{H}_{\text{ext}}] \quad (1.9)$$

Here  $\vec{H}$  is the local macroscopic field in the superconductor, where the microscopic field variations due to the vortex currents are averaged out.

Assuming the field and thus the vortex axis are in the z-direction,  $J$  is in the y-direction, Maxwells equation reduces to  $J_y = dH_z/dx$ . The expression for  $F_p(B,T)$  as a material constant of the individual super-conductor defines a "critical field gradient"

$$\left. \frac{dH}{dx} \right|_{\text{crit}} = J_c \quad (1.10)$$

If  $J_c$  and thus  $\left. \frac{dH}{dx} \right|_{\text{crit}}$  is exceeded, fluxlines or fluxline bundles overcome the pinning barriers and move in the opposite direction to the fluxoid density gradient  $dn/dx$ , with:

$$\left. \frac{dn}{dx} \right|_{\text{crit}} = \frac{\mu_0}{\phi_0} \left. \frac{dH_z}{dx} \right|_{\text{crit}} \quad (1.11)$$

until a new stable fluxoid arrangement is obtained.

Due to the same electrodynamic arguments which lead to the skin effect in a normal conductor, any change in the currents and thus the associated magnetic field always commence from the surface into the bulk superconductor.

In order to maintain the critical field gradient, (assuming a quasistationary case of slow  $\frac{dH_{\text{ext}}}{dt}$ ; the rising external field  $H_{\text{ext}}$  pushes the whole fluxfront into the superconductor as illustrated for a slab placed parallel to the field in Fig. (1.2a) for the simple (but unrealistic) case of field independent  $J_c$ . The interior of the superconductor is screened by supercurrents flowing in a layer of thickness  $x_p = H_{\text{ext}}/J_c$ .

Reducing  $H_{\text{ext}}$  below the peak value causes the fluxlines to move out of the superconductor, leading to an inverse critical field gradient and associated critical current density in the opposite direction. This condition is shown in Fig. (1.2b) for subsequent values of  $H_{\text{ext}}$  after a maximum value  $H_{\text{max}}$  with a penetration depth  $x_p$ , given by

$$H_{\text{max}} = \frac{dH_z}{dx} \cdot x_p = J_c x_p,$$

has been reached. A subsequent field rise yield a new pattern Fig. (1.2c) which is different from the initial behaviour shown in Fig. (1.2a).

This model for the magnetic behaviour of imperfect type II superconductors was first formulated by BEAN ) as critical state model. It postulates that depending on the history of the external field, the current density can only be zero in regions where never flux has penetrated, or it attains the critical value  $\pm J_c$ . Different to a normal conductor, regions of opposite flowing currents can coexist stationary in a superconductor.

For  $H_{\text{ext}}$  cycled between  $+H_{\text{max}}$  and  $-H_{\text{max}}$  the corresponding field patterns are given in Fig. (1.3). If a transport current is impressed on the superconductor, the fields at both sides of the conductor are essentially different and the current pattern is displaced such that a net current  $I_T$  remains, as illustrated in Fig. (1.4).

In the case of full field penetration i.e. if  $J_c \cdot d/2 \geq H_{\text{max}}$  is greater than the thickness  $d$  of the conductor, no field and current free regions exist.

## 1.2 Flux profiles

For a real type II superconductor the critical current density  $J_c$  is a function of  $H$  and  $T$ . The flux profile  $H(x)$ , (in the one dimensional case), is expressed as the solution of the differential equation

$$\frac{dH(x)}{dx} = \pm J_c (H(x)) \quad (1.11)$$

where the ( $\pm$ ) sign depends on the direction of  $J_c$ .

For constant  $J_c$  the linear field profile given in Fig. (1.2) and (1.3) (BEAN-model) is obtained.

A better approximation to the distribution of the current density in a real type II superconductor is given by using the KIM<sup>5)</sup> model, which relates the critical current density in the superconductor, to the local magnetic field by:

$$J_c = \frac{J_o H_o}{H + H_o} \quad (1.12)$$

where  $J_o$  and  $H_o$  are material constants.

Combining Eq. (1.11) and Eq. (1.12), we obtain:

$$\frac{dH}{dx} = \pm \frac{J_o H_o}{H + H_o} \quad (1.13)$$

Integrating Eq. (1.13) and noting, that at  $x = 0$ ,  $H(0) = H_{ext}$ , we get the equation for the field profile in an imperfect type II superconductor

$$H(x) = H_o \left\{ \left[ \left( 1 + \frac{H_{ext}}{H_o} \right)^2 - \frac{2\mu_o J_o \cdot x}{H_o} \right]^{1/2} - 1 \right\} \quad (1.14)$$

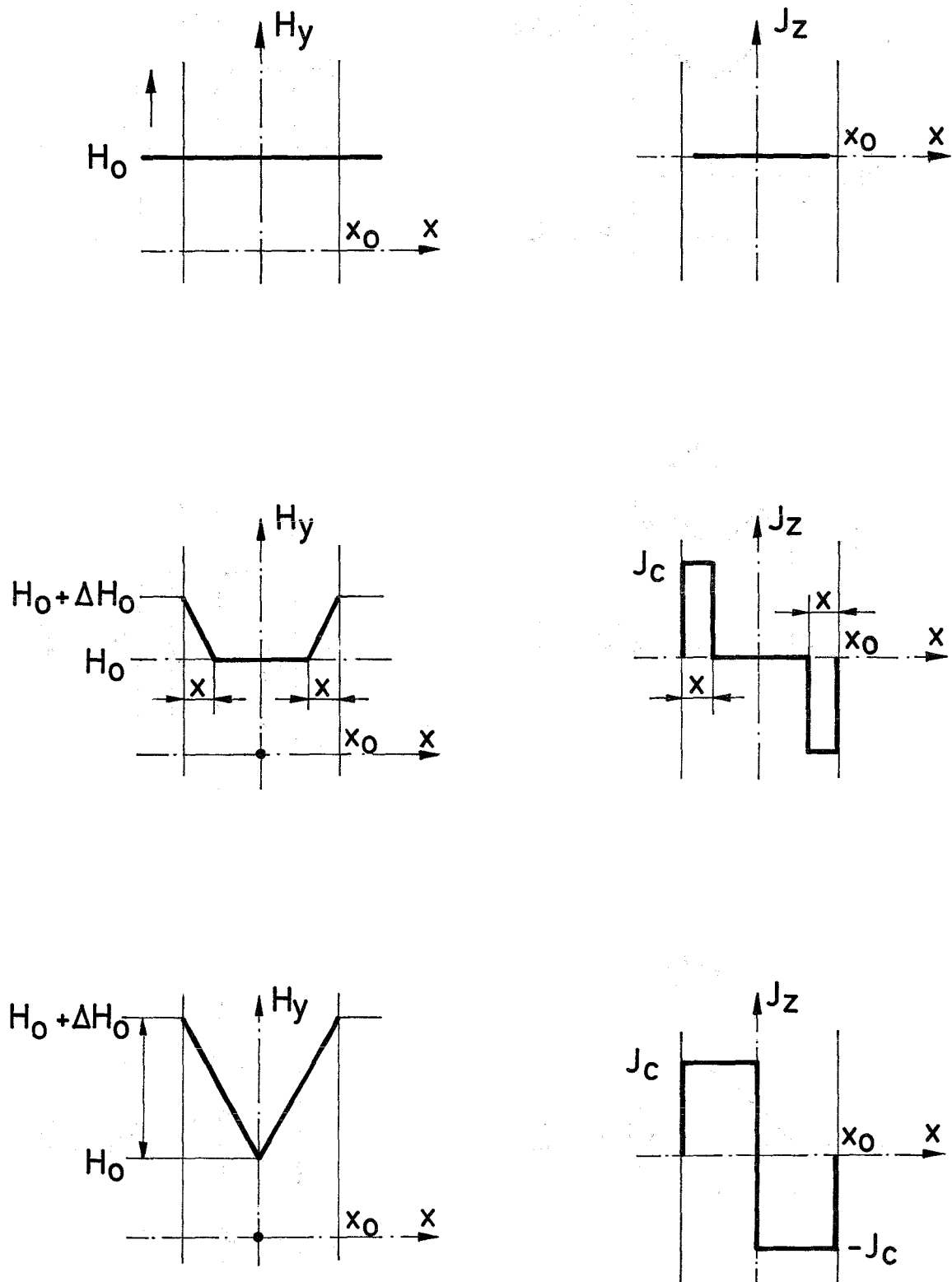


Fig.1.3a

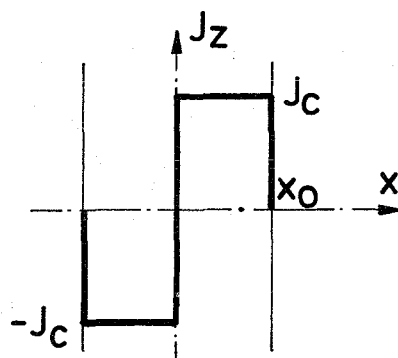
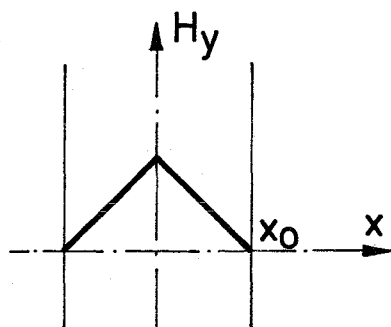
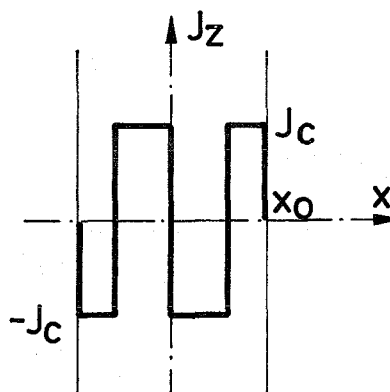
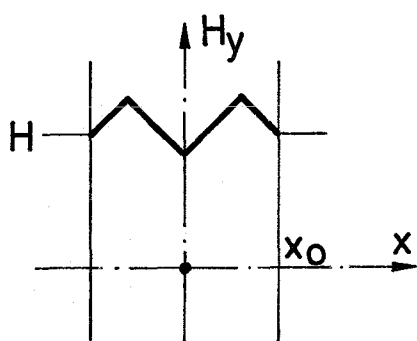
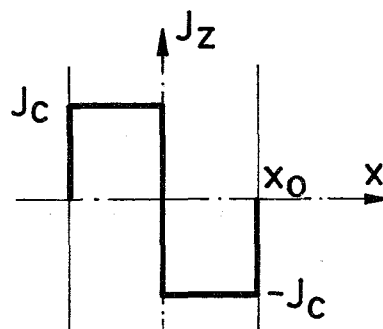
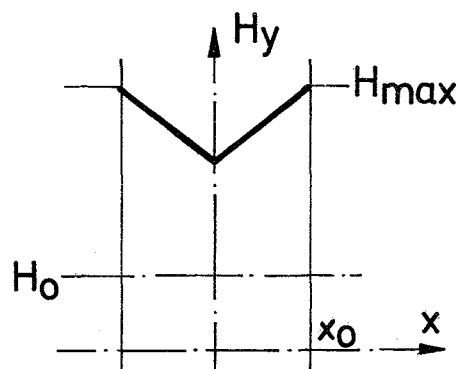


Fig.13b

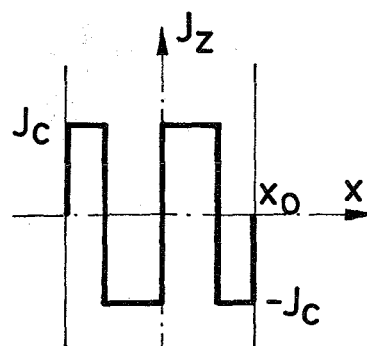
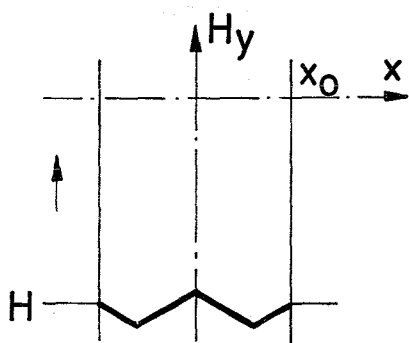
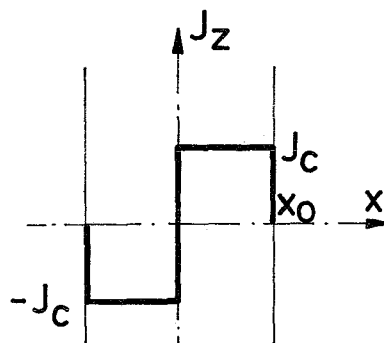
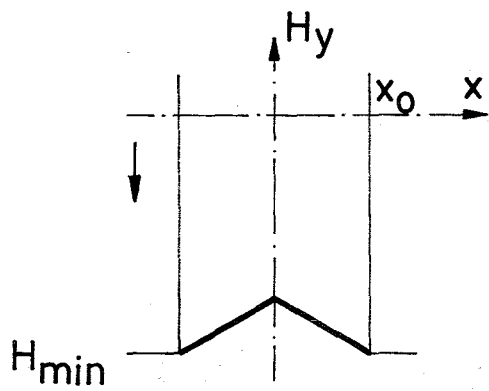
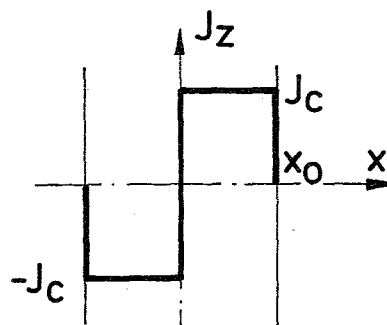
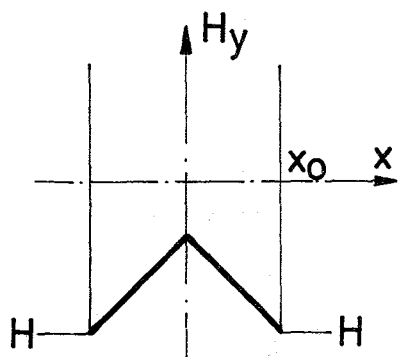


Fig.1.3c

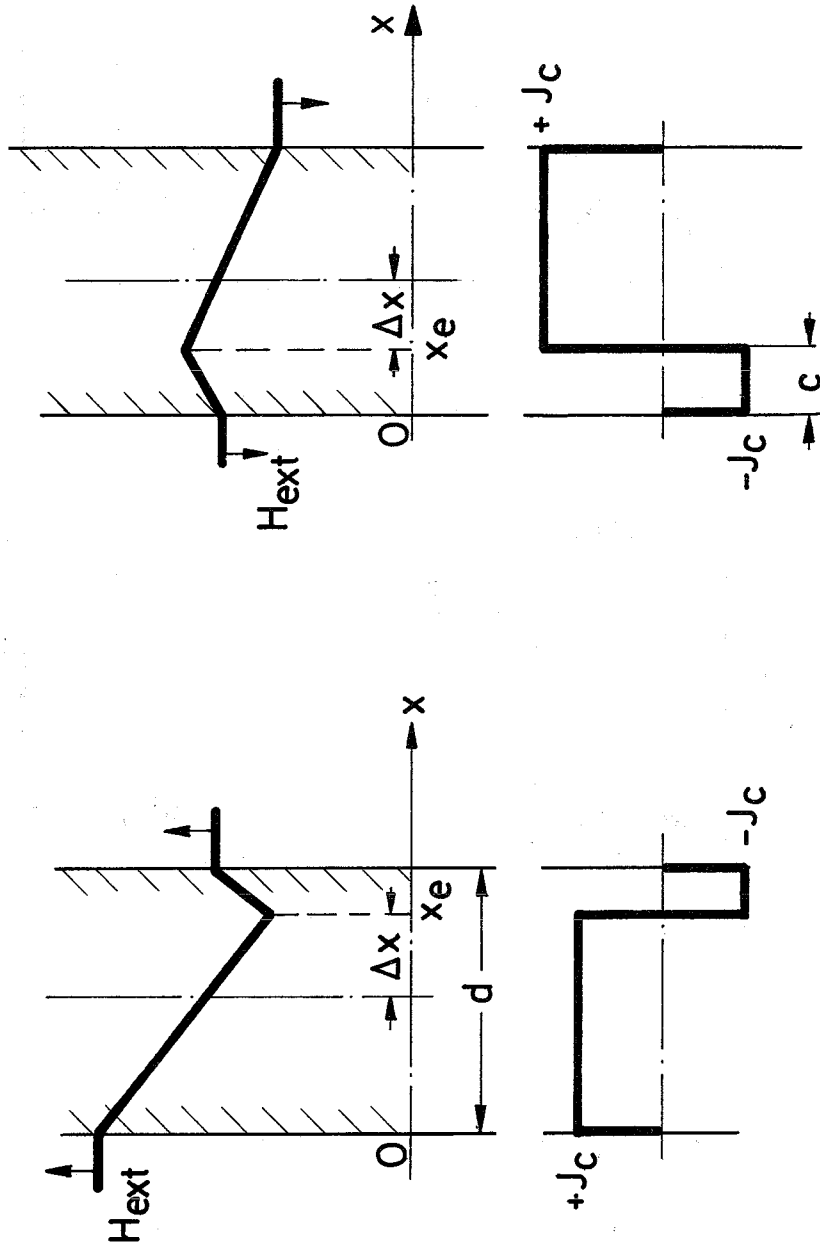


Fig.14

The distance from the surface at which H has dropped to zero is given by:

$$x_p = \frac{H_{\text{ext}}}{J_c H_0} \left[ \frac{1}{2} H_{\text{ext}} + H_0 \right] \quad (1,15)$$

Fig. (1.5) illustrates the field profile in a slab for increasing and decreasing external magnetic fields parallel to the surface of the slab.

### 1.3 Thin superconductors

For superconducting probes with a small thickness  $d$ , the external field penetrates into the whole conductor and is screened only partly in the middle of the conductor by an amount  $\Delta H = \frac{d}{2} J_c$ .

Thus  $H(0) = H_{\text{ext}} \pm \Delta H$

If the condition

$$\Delta H \ll H_{\text{ext}}$$

holds, i.e. the conductor thickness is

$$d \ll \frac{2H_{\text{ext}}}{J_c},$$

then  $J_c(H)$  can be replaced by  $J_c(H_{\text{ext}})$  and the approximation to a linear field profile in the superconductor is valid.

This is always satisfied for multifilament wires, where fine superconducting filaments (5...50 $\mu\text{m}$ ) are embedded in a normal metal matrix. With typical values of  $d = 10\mu\text{m}$  and  $J_c = 2 \cdot 10^5 \text{ A/cm}^2$ , we get  $\Delta H = 100 \text{ A/cm}$ , where as the external field in a superconducting magnet is in the range of several  $10^4 \text{ A/cm}$ .

#### 1.4 Finite size slabs and cylindrical conductors located in a transverse external field.

In the one dimensional model stated above,  $\text{curl } \vec{H}$  was expressed by  $\frac{dH_z}{dx}$  and all the other contributions were assumed to be zero. This is only true for an infinitely extended slab with a surface parallel to the (uniform) external field. In all other conductor configurations the magnetization currents distort the field and the current configuration in a complicated manner and cannot be treated by elementary methods. The case of a thin strip conductor with its face perpendicular to the field was evaluated by Morgan<sup>6)</sup>.

Clearly the one dimensional model as described, remains only a good approximation, as long as the curvature of fieldlines inside and outside of the conductor can be neglected, which is true if the screening field fulfills the condition

$$\Delta H = J_c \frac{d}{2} \ll H_{\text{ext}}$$

This condition holds always for multifilamentary conductors used for a.c. magnet applications.

#### 1.5 Methods of calculating hysteretic losses due to alternating fields.

For an imperfect type II superconductor located in a varying external field, the critical state model has the consequence of a varying magnetic flux in the material. (Fig. 1.5)

The changing flux must essentially penetrate the conductor surface and generates "hysteretic losses" due to the motion of flux lines.

The dissipative mechanism in a moving flux line is not well understood, but as the energy loss results entirely from the

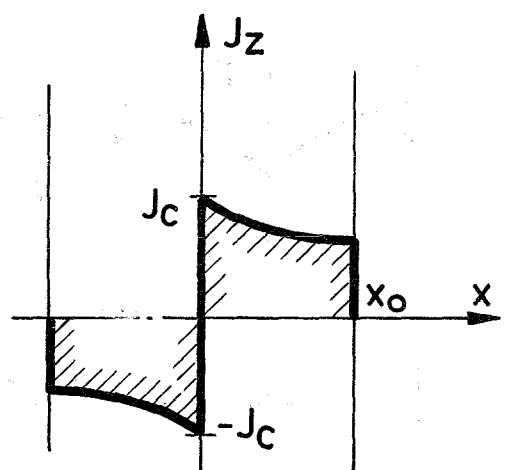
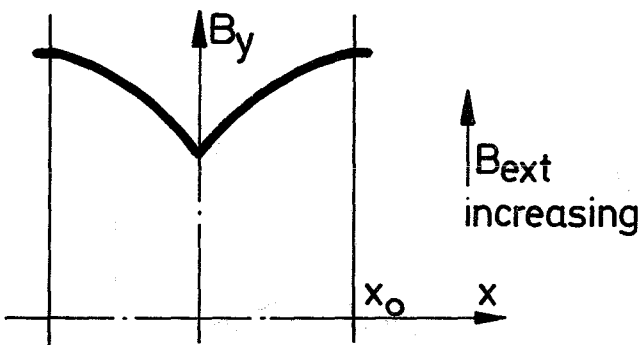
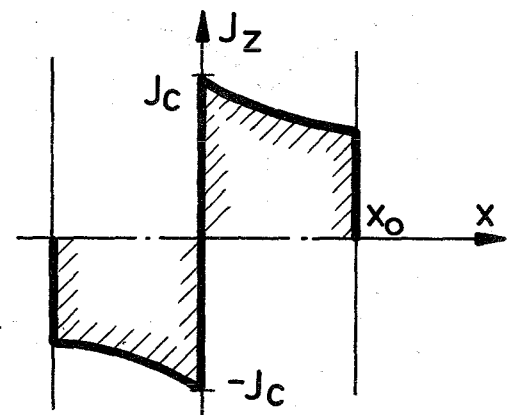
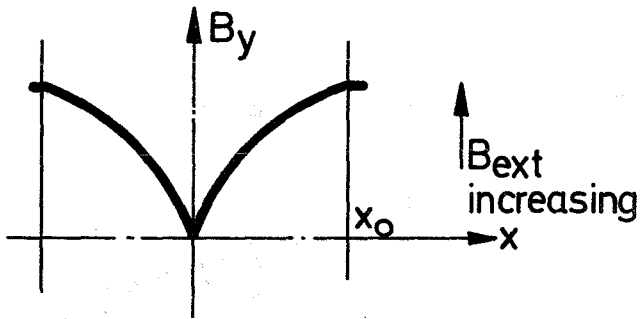
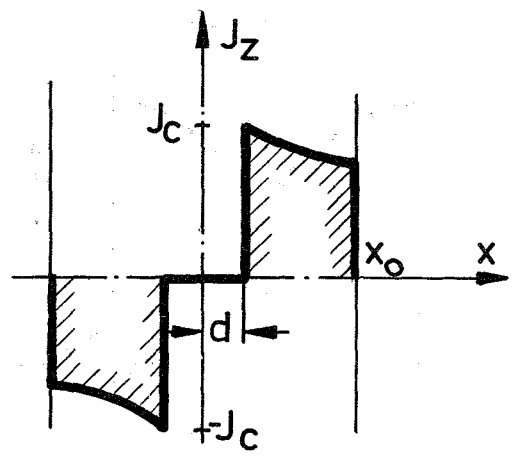
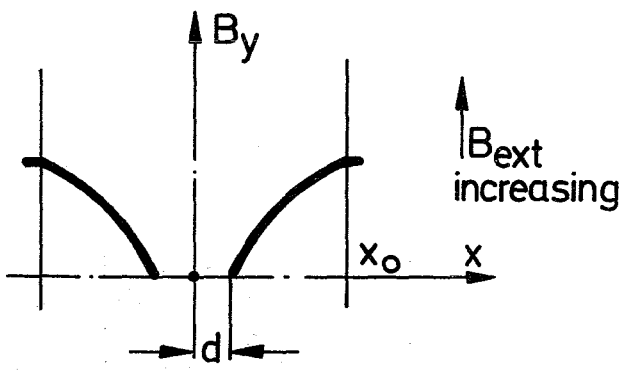


Fig.15a

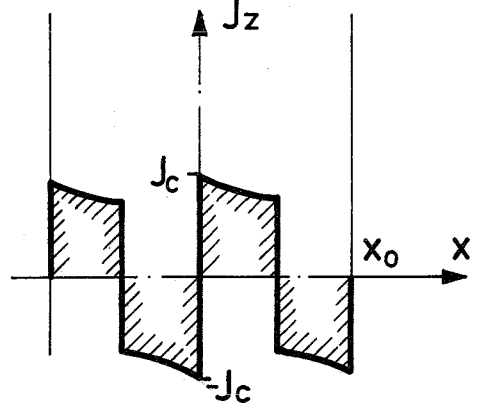
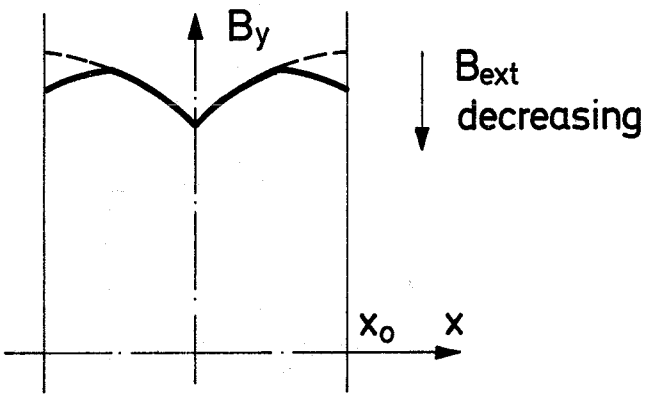
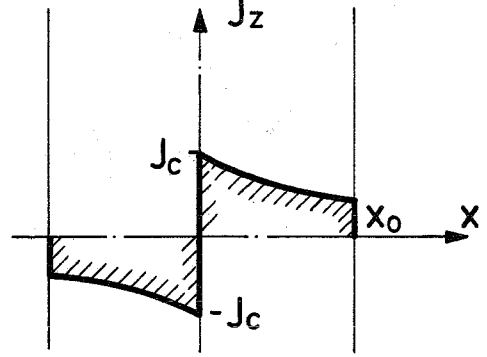
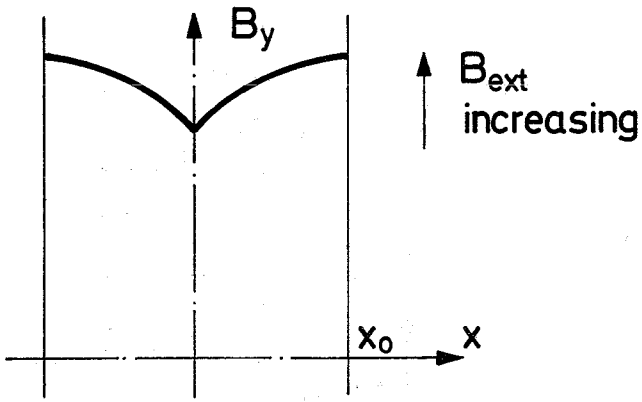
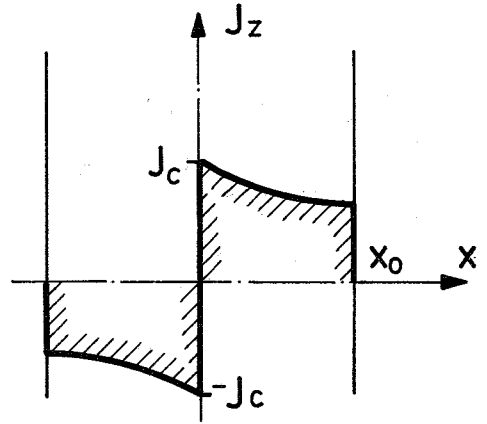
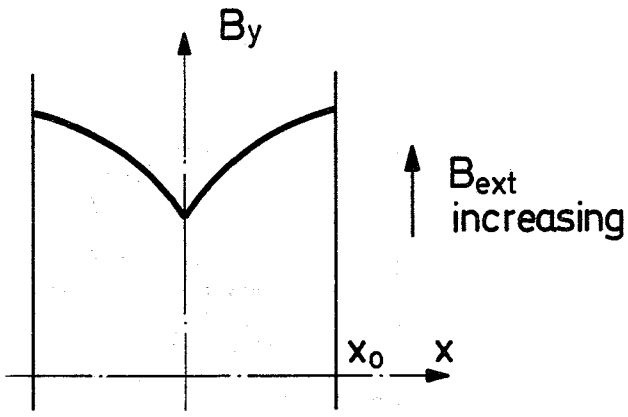


Fig.15b

magnetic field, loss computation is equivalent to evaluation of the electromagnetic energy dissipated during cycling of the field. Different approaches to solve this problem must essentially yield a unique result as they describe the same physical process:

- a) Integration of the Poynting vector  $\vec{S} = \vec{E}_s \times \vec{H}$  over the conductor surface and one cycle. The electrical field  $\vec{E}_s$  is given by the induction law  $\text{curl } \vec{E} = -\dot{\vec{B}}$
- b) Integration of Joule's energy  $\int \vec{J}_c \cdot \vec{E}$  over the conductor volume where  $\vec{E}$  has the same origin as in (a).
- c) Evaluation of the area under the magnetization curve for a full cycle  $\oint M(H) dH dV$ , where  $M$  is the magnetization due to currents  $\pm I_c$  in the sample.
- d) Volume integration of the mechanical work performed to the moving flux line lattice by the Lorentz force. The power loss per volume is expressed by  $p_v = (\vec{J}_c \times \vec{B}) \cdot \vec{v}$ , where  $\vec{v}$  is the velocity of the moving fluxoids and can be obtained by using the conservation law for the flux line density  $\text{div} (|\vec{B}| \cdot \vec{v}) = \dot{B}$ .

### 1.6 Hysteretic losses in slabs

For the simplest case, that the critical current density is independent of the magnetic field within the conductor, BEAN calculated hysteretic losses in slabs parallel to the external field. In his computation the transport current is not considered.

The field penetrates from both sides into the slab of thickness  $d$ . Full field penetration is obtained at

$$H_s = J_c \cdot \frac{d}{2} \quad (1.16)$$

For a probe exposed to a variable external field  $H_{ext}$ , cycled between the two values of  $-H_{max}$  and  $+H_{max}$ , we may distinguish between two cases:

a) Incomplete fluxpenetration:  $H_{max} < H_s$ ;

Integrating the magnetization  $\oint MdHdV$  over one cycle, the hysteretic losses can be expressed by

$$W_{hl} = \mu_0 V \cdot \frac{2}{3} \frac{H_{max}^3}{H_s} \quad (1.17)$$

$$W_{hl}/A = \mu_0 \frac{4}{3} \cdot \frac{H_{max}^3}{J_c} \quad (1.18)$$

With  $V$  the volume and  $A$  the area of the slab. In each half section of the slab the losses  $W_{hl}/2$  are dissipated.

b) Complete fluxpenetration:  $H_{max} \geq H_s$ ;

In this case no current free region exists in the slab.

Integration of the magnetization yields:

$$W_{hl} = 2\mu_0 H_s H_{max} V \cdot \left[ 1 - \frac{2}{3} \frac{H_s}{H_{max}} \right] \quad (1.19)$$

For field values:  $H_{max} \gg H_s$  this equation reduces to:

$$W_{hl} = \mu_0 d J_c H_{max} V \quad (1.20)$$

If however the external field is cycled between the values 0 and  $+ H_{\max}$  we obtain:

$$W_{hl} = \frac{\mu_0 d}{2} \cdot J_c \cdot H_{\max} V \quad (1.21)$$

For real superconductors the case of  $J_c$  independent of field is unrealistic. The more realistic model assumes the current density being dependent of field according to Kim<sup>5)</sup>:

$$J_c(H) = \frac{J_0 H_0}{H + H_0} \quad (1.12)$$

For this particular case the field profile within the conductor was given by the Eq. (1.14) and Fig. (1.5).

If the external field is swept in the range between  $H_{\max}$  and  $H_{\min}$ , the corresponding field values within the superconductor can be obtained from the equation:

$$H^2 + 2H_0 \cdot H - H_{\text{ext}}^2 - 2H_0 \cdot H_{\text{ext}} \pm 2J_0 H_0 x = 0,$$

and shown in Fig. (1.6) for ascending and descending  $H_{\text{ext}}$ . The relation between the local field  $H$  and the distance from the slab surface is given by

$$x = \pm \frac{1}{2J_0 H_0} \left[ (H + H_0)^2 - (H_{\text{ext}} + H_0)^2 \right]$$

The two branches of the field extending from  $H_{\text{ext}}$  on the surface of the slab to  $P_1$  and  $P_3$  correspond to field values of

$$H > H_{\text{ext}} \quad (\text{Descending field})$$

$$H < H_{\text{ext}} \quad (\text{Ascending field})$$

The penetration differences in the three regions I-III are given by:

$$\Delta x_I = \frac{1}{2J_0 H_0} \left[ 2(H + H_0)^2 - (H_{\text{ext}} + H_0)^2 - (H_{\text{max}} + H_0)^2 \right]$$

$$\Delta x_{II} = \frac{1}{2J_0 H_0} \left[ (H_{\text{max}} + H_0)^2 - (H_{\text{ext}} + H_0)^2 \right]$$

$$\Delta x_{III} = \frac{1}{2J_0 H_0} \left[ 2(H + H_0)^2 - (H_{\text{ext}} + H_0)^2 - (H_{\text{min}} + H_0)^2 \right]$$

Introducing the abbreviations:

$$h = H + H_0; h_{\text{ext}} = H_{\text{ext}} + H_0; \text{ etc. and}$$

$$h_1 = \frac{1}{\sqrt{2}} (h_{\text{ext}}^2 + h_{\text{max}}^2)^{\frac{1}{2}}; h_2 = \frac{1}{\sqrt{2}} (h_{\text{max}}^2 + h_{\text{min}}^2)^{\frac{1}{2}}$$

$$h_3 = \frac{1}{\sqrt{2}} (h_{\text{ext}}^2 + h_{\text{min}}^2)^{\frac{1}{2}},$$

we may write for the irreversible part of the magnetization:

$$\begin{aligned} \Delta M = & \frac{1}{2J_0 H_0} \int_{h_1}^{h_{\text{ext}}} (2h^2 - h_{\text{ext}}^2 - h_{\text{max}}^2) dh + \frac{1}{2J_0 H_0} \int_{h_{\text{ext}}}^{h_2} (h_{\text{max}}^2 - h_{\text{ext}}^2) dh \\ & + \frac{1}{2J_0 H_0} \int_{h_2}^{h_3} (h^2 - h_{\text{ext}}^2 - h_{\text{min}}^2) dh \end{aligned}$$

which after integration and rearrangement is written in the form:

$$\Delta M = \frac{1}{2J_0 H_0} \left[ \frac{2}{3} h_{\text{ext}}^3 + \frac{\sqrt{2}}{3} (h_{\text{ext}}^2 + H_{\text{max}}^2)^{\frac{3}{2}} - \frac{\sqrt{2}}{3} (h_{\text{ext}}^2 + h_{\text{min}}^2)^{\frac{3}{2}} + \frac{\sqrt{2}}{3} (h_{\text{max}}^2 + h_{\text{min}}^2)^{\frac{3}{2}} - 2h_{\text{ext}} \cdot h_{\text{max}}^2 \right] \quad (1.22)$$

As usual we calculate the hysteretic losses from

$$W_{hl} = \mu_0 \int_{H_{\text{min}}}^{H_{\text{max}}} M dH_{\text{ext}} = \mu_0 \int_{h_{\text{min}}}^{h_{\text{max}}} M dh_{\text{ext}}$$

and obtain the hysteretic losses per unit surface for a semi-infinite slab.

$$W_{hl} = \frac{\mu_0}{2J_0 H_0} (H_{\text{min}} + H_0)^4 \left[ f^4 \left( \frac{1}{4} + \frac{1}{4\sqrt{2}} \frac{1+\sqrt{1+f^2}}{(1+\sqrt{2})f} - \left( \frac{5}{12} - \frac{1}{4\sqrt{2}} \frac{f+\sqrt{1+f^2}}{1+\sqrt{2}} \right) - f^2 - \frac{\sqrt{1+f^2}}{6\sqrt{2}} \left( 3f^2 - \frac{13}{2}f^2 + \frac{3}{2}f - 5 \right) \right] \quad (1.23)$$

$$\text{with } f = \frac{H_{\text{max}} + H_0}{H_{\text{min}} + H_0}$$

It may be pointed out that Eq. (1.22) is true only, if  $H_{\text{max}}$  and  $H_{\text{min}}$  have the same sign, as the analytical expression for  $J_c(H)$

is valid only for  $H > 0$ .

Eq. (1.22) is particularly useful to calculate losses in superconducting magnetic shields (incomplete penetration).

### 1.7 Application to multifilament conductors:

Superconductors used for a.c. applications have diameters in the  $\mu\text{m}$  range. For these superconductors the case of complete flux-penetration is valid.

As seen in (1.2) the assumption of  $\Delta H \ll H_{\text{ext}}$  implies that linear field penetration is valid and the equations derived from Bean's model are correct for slabs of finite size as well as for cylindrical conductors as shown in (1.2) and (1.3).

We regard a slab, located parallel to the external field  $H_{\text{ext}}$ , having a thickness  $d$  and a high  $b$ . A net transport current  $I_T$  is now admitted to pass through the slab. The electric center of the slab<sup>†</sup> which was identical to the geometric center of the slab for  $I_T=0$  is displaced due to the transport current by a distance:

$$\Delta x = \frac{d}{2} \cdot \frac{I_T}{I_c} \quad (1.24)$$

The displacement is illustrated in Fig. (1.4a,b) for increasing and decreasing fields. At points of field reversal, the simple field pattern is modified. These field perturbations modify the hysteretic losses, as written in Eq. (1.18). The additional loss contribution in this equation can be neglected only if  $\Delta H \ll H_{\text{max}}$ .

Obviously for  $\Delta x = \frac{d}{2}$  the critical current of the probe is attained, beyond which steady flux flow occurs across the superconductor. The power density dissipated in the superconductor is calculated for the case, that the external field changes with  $\dot{H}_{\text{ext}}$  from

$$P = \vec{E} \cdot \vec{J}$$

---

<sup>†</sup> The electric center is defined as a plane within the conductor separating the two regions of opposite flowing  $J_c$ .

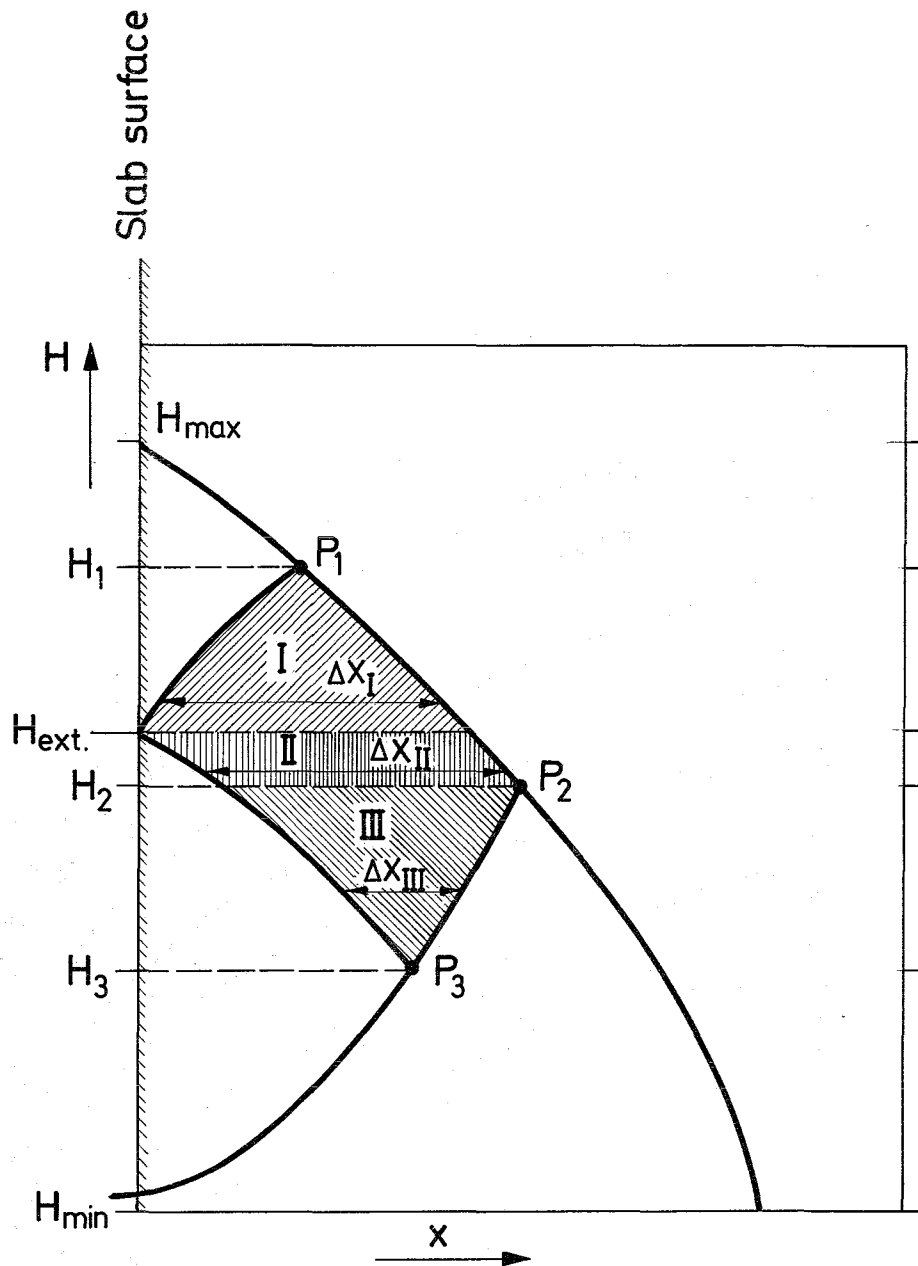


Fig.16

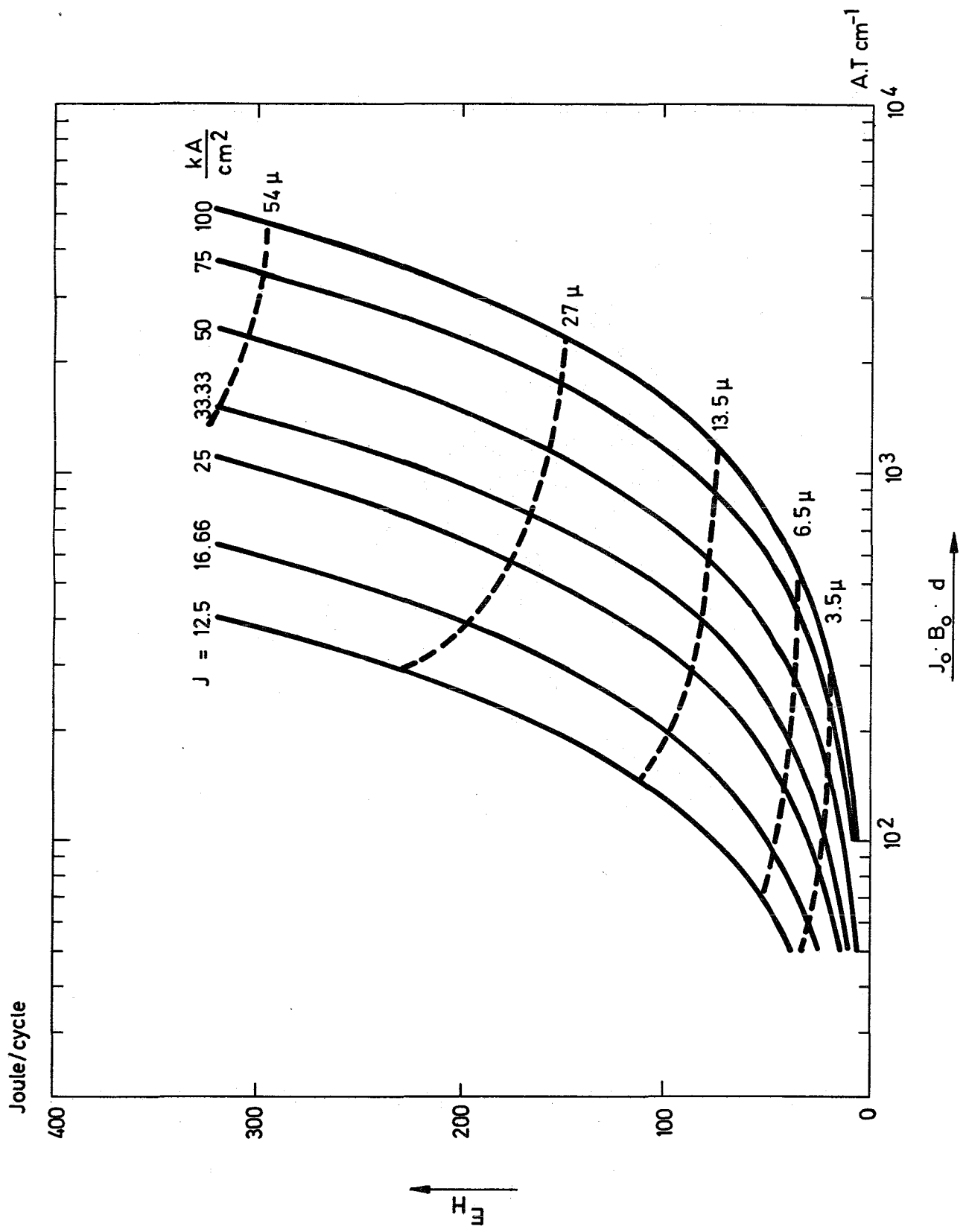


Fig.17

For our particular geometry,  $\vec{H} = H_z$ ;  $\vec{J}_c = J_y$ ;  $\vec{F}_L = F_{Lx}$ , and Maxwell's law for the electrical field curl  $E = -\dot{B}$  yield

$$\frac{dE_y}{dx} = -\mu_0 \dot{H}_{ext} \cdot (x-x_e)$$

where the internal field change  $H_z(x)$  can be set approximately as  $H_{ext}$  for thin probes. As at the electrical center  $x_e$ , the fluxline velocity is zero, the axial electric field  $E_y(x_e)$  must vanish.  $E_y$  is obtained by simple integration with one boundary being  $x_e$ .

$$E_y(x) = -\mu_0 \dot{H}_{ext} \cdot (x-x_e) \quad (1.25)$$

The sign of  $J_y$  is given by the position and sense of the field change

$$J_y = \begin{cases} + J_c \text{ for } x < x_e; \dot{H} > 0 \text{ or } x > x_e; \dot{H} < 0 \\ - J_c \text{ for } x < x_e; \dot{H} < 0 \text{ or } x > x_e; \dot{H} > 0 \end{cases}$$

Thus the energy dissipation rate per conductor length is given by:

$$\frac{P_{hl}}{l} = \mu_0 b J_c \dot{H}_{ext} \int_0^d (x-x_e) dx \quad (1.26)$$

The integral yields after introducing  $x_e = \frac{d}{2} + \frac{I_T}{2J_c b}$ , and the slab volume  $V = b \cdot l \cdot d$ , the conductor losses:

$$P_{hl} = \mu_0 V J_c \cdot \frac{d}{3} \cdot |\dot{H}_{ext}| \cdot \left[ 1 + \left( \frac{I_T}{I_c} \right)^2 \right] \text{ (Watt)} \quad (1.27)$$

where  $I_c = b \cdot d \cdot J_c$  is the critical short sample current at the corresponding field.

Hysteretic losses are usually related to one cycle if  $H_{ext}$  is changed periodically between field values  $H_{min}$  and  $H_{max}$  such as:  $H_{min} \rightarrow H_{max} \rightarrow H_{min}$ .

The losses per cycle are independent of frequency and wave form, the only material property entering the loss equation is the  $J_c(H)$ -dependence.

$$\Delta W_{hl} = \frac{\mu_0}{2} V d \int_{H_{min}}^{H_{max}} J_c(H) \left[ 1 + \left( \frac{I_T(H)}{I_c(H)} \right)^2 \right] dH \quad (1.27)$$

The term  $I_T/I_c$  depends on the particular magnet and contributes only at the peak current value to the losses in the high field region of a coil. Usually the term is small and can be neglected. Kim's model relating the critical current and field is a good approximation for type II multifilamentary conductors. entering  $J_c$  from Eq. (1.12) in Eq. (1.27), we obtain the well known formula for hysteretic losses in superconductors with small diameters:

$$W_{hl} = \frac{\mu_0 J_c H_0 V}{2} d \cdot \ln \left( \frac{H_{max} + H_0}{H_{min} + H_0} \right) \quad \left( \frac{Ws}{cycle} \right) \quad (1.28)$$

$V$  is the total volume, if  $J_c$  is referred to as the overall current density of the conductor or it is the volume of the superconductor, if  $J_c$  is the current density in the superconductor.

If field reversal occurs during the field sweep. i.e. if for instance  $H_{min}$  is negative, the losses have to be split into two parts: Losses in the region:  $0 \rightarrow H_{max} \rightarrow 0$  and losses in the region  $0 \rightarrow H_{min} \rightarrow 0$ .

Thus the total losses are given by:

$$W_{hl} = \frac{\mu_0 J_c H_0 V}{2} \cdot d \cdot \ln \frac{(H_{\max} + H_0) \cdot (H_{\min} + H_0)}{H_0^2} \quad (1.29)$$

### 1.8 Hysteretic losses in cylindrical shaped superconductors

The above loss calculations for slab geometries are simple, but not correct when applied to magnets using composite conductors with superconducting tapes embedded in normal metal strips. As the field over the length of the tape is not always parallel to the surface of the superconductor, this type of conductor is not utilized in pulsed magnets due to enhanced dissipative losses.

The loss calculations are specifically applicable to cylindrical shaped filamentary conductors. Coextruded superconductor and copper wires result generally in superconducting filament shapes having more or less circular cross sections. If the superconducting filament is distorted during extrusion the use of the hydraulic diameter ( $d = \frac{4A}{P}$ ) in the calculation is a good approximation to obtain losses in superconductors, where A denotes the cross section and P the perimeter of the filament. With the restriction to thin filaments with a diameter of  $\frac{J_c d}{2} \ll H_{\text{ext}}$  and  $I_T \ll I_c$  (valid for nearly the whole field sweep), the integration of the product (J.E) over a cylinder is performed by Morgan<sup>6)</sup> in cylindrical coordinates. Starting with curl  $\vec{E} = -\mu_0 \frac{dH_{\text{ext}}}{dt}$ , in cylindrical coordinates (r,θ), we have

$$\frac{1}{r} \frac{\partial E_z}{\partial \theta} = -\mu_0 \cdot \frac{\partial H_r}{\partial t} \quad (1.31)$$

and:

$$\frac{\partial E_z}{\partial r} = \mu_0 \cdot \frac{\partial H_\theta}{\partial t} \quad (1.32)$$

$H_r$  and  $H_\theta$  are expressed by  $H_{ext}$  in the case of a symmetric flux profile with  $\Delta x = 0$ .

With  $\frac{\partial H_r}{\partial t} = \sin(\theta) \cdot \dot{H}_{ext}$ , and  $\frac{\partial H_\theta}{\partial t} = \cos(\theta) \cdot \dot{H}_{ext}$

one obtains: 
$$\frac{1}{r} \frac{\partial E_z}{\partial \theta} = -\mu_0 \sin(\theta) \cdot \dot{H}_{ext} \quad (1.33)$$

and: 
$$\frac{\partial E_z}{\partial r} = \mu_0 \cos(\theta) \cdot \dot{H}_{ext} \quad (1.34)$$

The solution of Eq. (1.34)

$$E_z = \mu_0 \cdot r \cdot \cos(\theta) \cdot \dot{H}_{ext} \quad (1.35)$$

gives the field distribution within the cylinder.

The power loss is given by:

$$P_{hl} = \vec{E} \cdot \vec{J} \cdot dV = E_z \cdot J_c \cdot dV$$

where  $E_z$  is always directed along  $J_z = \pm J_c$

Substituting  $E_z$  from Eq. (1.35) in  $P_{hl}$  we obtain for a conductor of length  $l$

$$P_{hl} = 2\mu_0 J_c \dot{H}_{ext} \cdot l \int_0^{d/2} \int_{-\pi/2}^{\pi/2} r^2 \cos(\theta) dr d\theta$$

$$P_{hl} = \frac{8}{3\pi} \mu_0 V J_c \frac{d}{4} \cdot \dot{H}_{ext} \quad (1.36)$$

With  $d$  the diameter of the superconductor and  $V$  its volume:

The energy loss is given by the time integral of Eq. (1.36). Comparison with the corresponding Eq. (1.27) for a slab shaped conductor shows that hysteretic losses in a cylindrical conductor are less by a factor  $8/3 \pi \approx 0.85$ , than in a slab of the same volume i.e. the same current carrying capacity and thickness.

The factor  $\frac{8}{3\pi}$  in Eq. (1.36) occurs in all loss equations for cylindrical geometries.

At a low frequency field sweep ( $\leq 1\text{Hz}$ ), hysteretic losses are the main contributor among the losses encountered in the conductor. To evaluate hysteretic losses per cycle for the entire coil Eq. (1.29) must be integrated over the coil volume. As  $H_{\max}$  and  $H_{\min}$  occur in logarithmic form, the losses per cycle can be obtained with good accuracy (about 20%), if  $H_{\max}$  and  $H_{\min}$  are replaced by the mean field values over the entire coil.

Fig. (1.7) illustrates calculated hysteretic losses for a pulsed superconducting dipole magnet. The aperture field of the magnet is cycled from zero to 5T. The coil cross-section is an approximation of intersecting ellipses and the magnet has an aperture of  $8 \times 11 \text{ cm}^2$  and a length of 100 cm. In the abscissa the term  $J_0 H_0 d$  contains all relevant conductor parameters.<sup>+</sup> As for  $\mu_0 H_0$  a typical value of 1T is used in the calculation. The losses for different peak current densities (at 5T) are represented by the solid lines. As the conductor volume decreases with increasing current carrying capacity  $J_0 H_0$ , we see that the total losses proportional to  $J_0 H_0$  are not a strong function of the  $J_0 H_0$  parameter for a given magnet.

This loss dependance is shown by the broken line with the filament diameter  $d$  as a parameter, where we have assumed that the current density at 5T attains just the critical value.

---

<sup>+</sup> Twisted multifilament conductor is assumed.

From the presented analysis and the curves of Fig. (1.7) it is seen that the most promising attempt to reduce a.c. losses is in using thin filaments in the conductor. NbTi filaments having individual diameters of  $\leq 5\mu\text{m}$  are commercially available. Several thousand of such filaments are drawn in a metallic matrix and are twisted. A number of such conductors (called composite conductors, or strands) are transposed to form a cable or braid for a.c. applications.

### 1.9 Hysteretic losses in coils using hollow superconducting filaments

It was possible to produce multifilament composites in long lengths (>1km) only by using NbTi. Nb<sub>3</sub>Sn and V<sub>3</sub> Ga has been used in multifilament composites of short length (100-300m). The  $\beta$ -tungsten series is brittle and production of composites has been restricted to short lengths due to manufacturing difficulties.

Alternate solution are sputtering of thin layers on glass filament carriers or some other suitable material. The losses of such a tubular conductor, having an inner diameter  $d_1$ , an outer diameter  $d_2$  are obtained from Eq. (1.37):

$$W_{hl} = \frac{\pi^2}{8} J_0 H_0 l_{sc} (d_2^3 - d_1^3) \ln \frac{H_m + H_0}{H_1 + H_0} \quad (1.37)$$

Dividing the losses by the volume of the superconductor

$$V_{sc} = \frac{\pi}{4} (d_2^2 - d_1^2) \cdot l_{sc}$$

and referring to the same current carrying capacity in the conductor, we find that  $W_{hl}/I_{Tmax}$  depend only on the ratio  $d_1/d_2$ :

$$\frac{W_{hl}}{I_{Tmax}} \sim \frac{d_2^3 - d_1^3}{d_2^2 - d_1^2} = d_2 \frac{1 - (d_1/d_2)^3}{1 - (d_1/d_2)^2} \quad (1.38)$$

Compared to a filament with  $d_1=0$ , losses are increased by the factor  $1 - (d_1/d_2)^3 / 1 - (d_1/d_2)^2$  for the same critical current density and identical total current.

### 1.10 Losses in Composites

Losses in superconducting coils, when exposed to time varying magnetic fields have several origins:

- Eddy Current losses in the conductor matrix.
- Self field losses.
- Hysteretic losses.
- Auxillary losses due to nonuniform magnetic fields.

In section (1.6) and (1.7) we had treated so far hysteretic losses. We discuss in the following the origin and the magnitude of the other losses occurring in a.c. coils. We consider however only twisted multifilament conductors.

### 1.11 Eddy Current losses in the conductor matrix:

In any metallic conductor eddy currents are induced if  $\dot{B} \neq 0$ . In a composite conductor these induced currents are modified by the superconducting filaments, which do not admit (first order observation) a resistive longitudinal component of the electrical field.

To calculate eddy current losses, the matrix material, the current distribution in the matrix depending on the conductor geometry, and the rate of field rise must be known. We assume uniform distribution of filaments throughout the composite,

and an external field perpendicular to the conductor axis, as is usually the case in coils:

a) We regard for the time being, only the outer layer of filaments embedded in a cylindrical composite. This layer has a radius  $D/2$  and the filaments are twisted with a pitch of length  $l_p$ .

The magnetic field  $B$  acting in the cylinder is assumed to be homogeneous and perpendicular to the axis of the composite<sup>+</sup>. The field is composed of the external field  $B_{ext}$  and an additional field  $B_e$  generated from induced currents in the filaments.

$$B = B_{ext} + B_e$$

The voltage induced in the conductor is obtained from the contourintegral (over  $C$ ) taken along the electric centers of two oppositely placed filaments as shown in Fig. (1.8 ).

$$\oint_C \vec{E} ds = - \dot{\Phi} = - \int \dot{B} dA = - 2D \sin \left( \frac{2\pi}{l_p} z \right) \cdot \dot{B} \frac{l_p}{2\pi} \quad (1.39)$$

This voltage must drop entirely in the two transverse passages  $\overline{1-2}$  and  $\overline{3-4}$  through the matrix. Relating the electrical potential  $V(z)$  of the filaments to the axis of the composite, it is seen that at the crossover point  $A$  at  $z = l_p/4$ , the potential  $V(z)$  must be a maximum. The voltage at  $z = 0$  must be zero because of the antisymmetric condition at  $z = 0$ .

At an arbitrary point the electrical potential is expressed by

$$V(z) = \frac{D}{2} \dot{B} \frac{l_p}{2\pi} \sin \left( \frac{2\pi}{l_p} z \right) \quad (1.40)$$

---

<sup>+</sup> The assumption of a uniform magnetic field is justified according to Eq. (1.46).

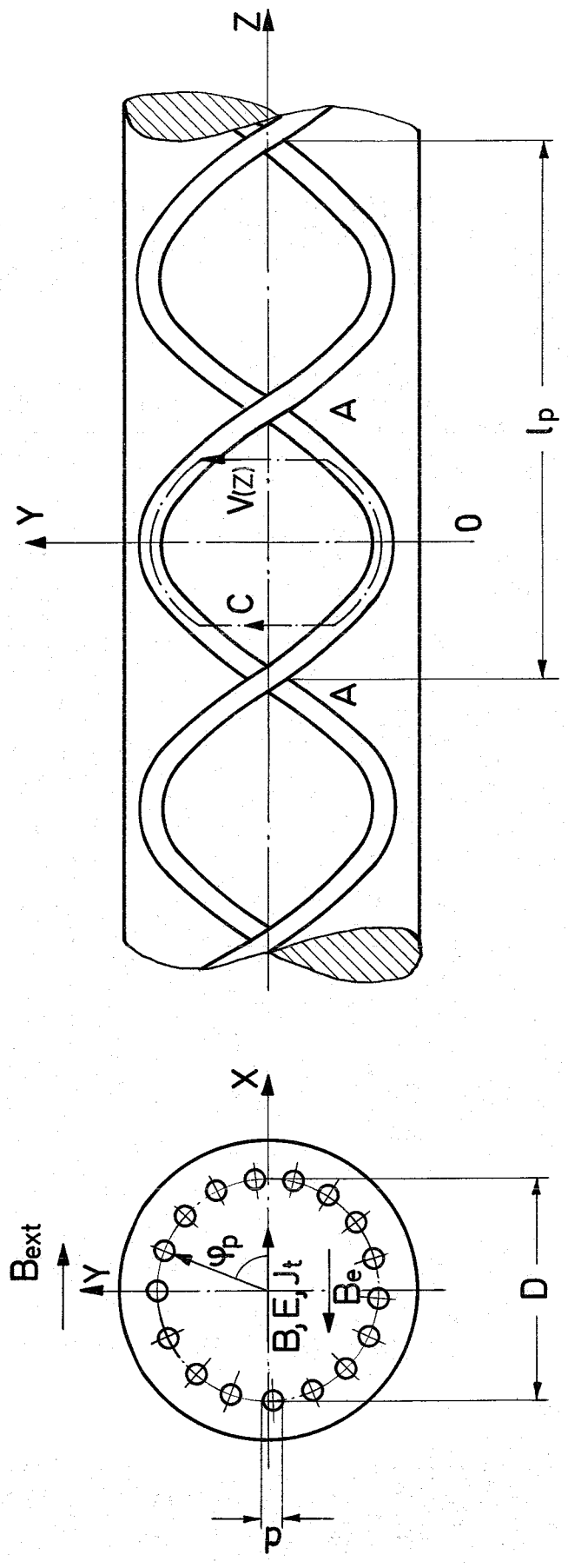


Fig. 1.8

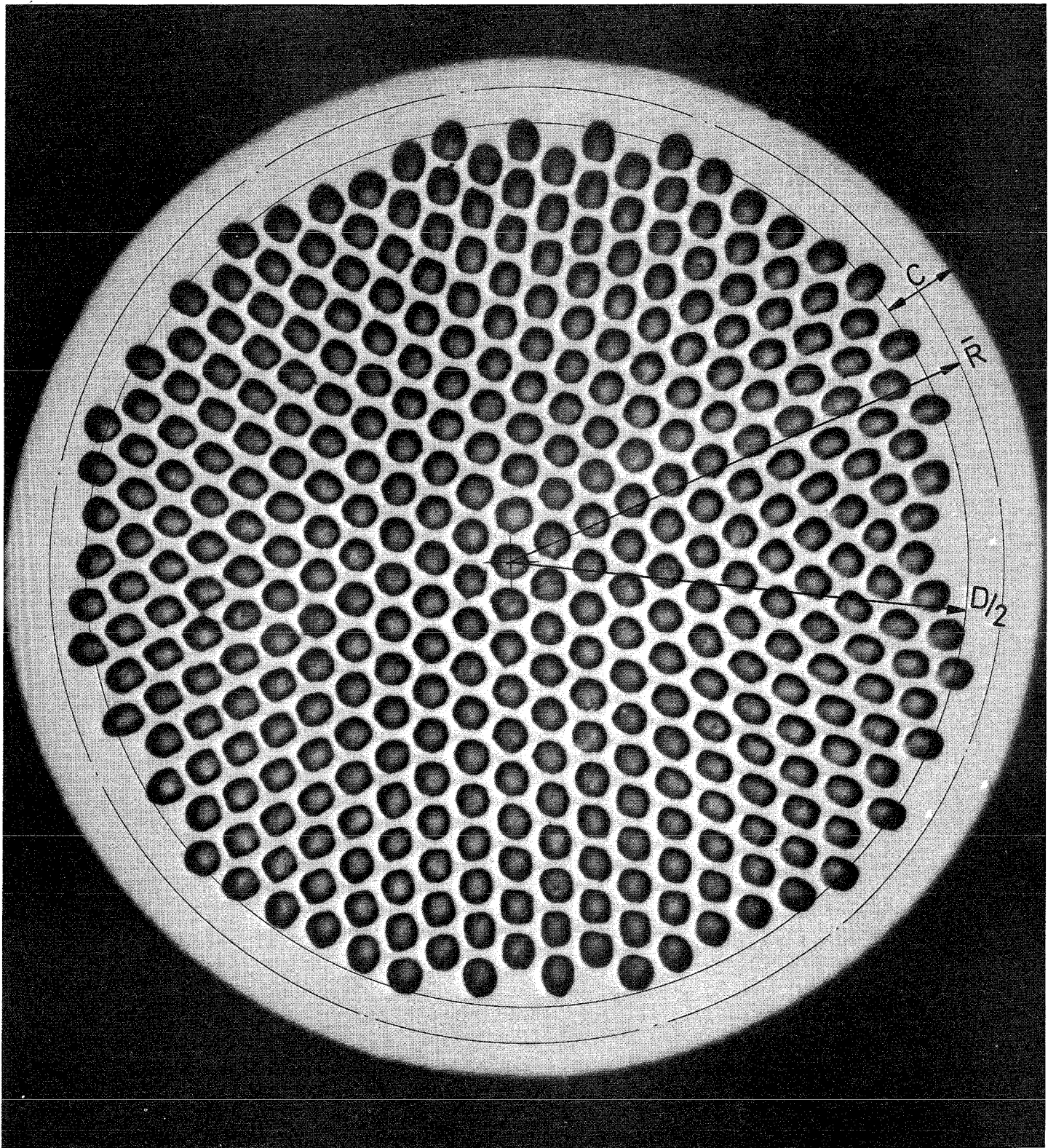


Fig. 1.9

as the potential between the conductor axis and one filament is just a quarter of the contourintegral Eq. (1.39).

$z$  can be expressed by the twist angle  $\varphi_p$  between the filament axis and the plane perpendicular to  $B$ ; i.e.  $\varphi_p = \pm \frac{2\pi}{l_p} z$ , where the sign corresponds to the sense of the twist. Thus we get for each single filament:

$$V(z) = \pm \dot{B} \frac{l_p}{2\pi} \cdot \frac{D}{2} \sin(\varphi_p) = \pm \dot{B} \frac{l_p}{2\pi} x \quad (1.41)$$

if the sense of  $\dot{B}$  is assumed to be in the  $x$  direction.

Eq. (1.41) is valid for each single filament in the outer layer. If we approximate the layer of filaments by an infinitesimal thin cylinder, then the boundary conditions for Eq. (1.41) are met by an homogeneous electric field in the cylinder in  $\dot{B}$ -direction.

$$E = E_x = \mp \dot{B} \left( \frac{l_p}{2\pi} \right) \quad (1.42)$$

The transverse current density in the composite is thus:

$$J_t = \mp \frac{1}{\bar{\rho}_c} \left( \frac{l_p}{2\pi} \right) \cdot \dot{B} \quad (1.43)$$

From these equations we obtain the eddy current losses per volume occuring within the filament bundle of diameter  $D$ :

$$p_e = \frac{1}{\bar{\rho}_c} E^2 = \frac{1}{\bar{\rho}_c} \left( \frac{\dot{B} l_p}{2\pi} \right)^2 \quad (1.44)$$

where  $\bar{\rho}_c$  is the effective transverse resistivity of the composite.

b) Only the outer layer of filaments in the cylindrical composite conductor was considered above. It was seen however from Eq. (1.42), that the diameter of the filament layer could be eliminated indicating that the electric field  $E_x$  is independent of  $D$ . Thus we may fill the entire composite cross-section with concentric layers of filaments and present a realistic model of a twisted multifilament conductor. As  $l_p$  is unchanged for all layers, the field configuration in the interior of the composite is not altered. However the transverse effective resistivity  $\bar{\rho}_c$  must be averaged properly over the conductor:

$$\bar{\rho}_c = \rho_{\text{matrix}} \cdot \left( \frac{w}{w-d} \right),$$

where  $d$  is the filament diameter,  $w$  the distance between the centers of adjacent filaments.

It is assumed here, however, that the eddy currents flow through the matrix material and do not cross superconducting filaments due to the relatively high resistance of the interface layer between superconductor and the matrix.  $\rho_{\text{matrix}}$  is the resistivity of the matrix material, including size effect, mechanical strain effects and longitudinal magnetoresistance.

In presently available composite conductors the filament bundle is still surrounded by a layer of "pure" matrix material of thickness  $C$  (see Fig. 1.9). The potential  $V(\varphi_p)$  in Eq. (1.41) causes additional eddy currents in this part of the conductor and the associate losses  $P'_e/l$  per conductor length are given by

$$\frac{P'_e}{l} = \int_0^{2\pi} \bar{R} d\varphi_p \cdot \left( \frac{dV(\varphi_p)}{R d\varphi_p} \right)^2 \cdot \frac{C}{\rho_{\text{matrix}}} = \frac{\pi D^2}{4} \left( \frac{B l_p}{2\pi} \right)^2 \cdot \frac{C}{R} \cdot \frac{1}{\rho_{\text{matrix}}}$$

Eddy current losses for a cylindrical composite are thus given by

$$\frac{P_e}{I} = \frac{\pi}{4} \cdot D^2 \left( \frac{B_1}{2\pi p} \right)^2 \left( \frac{w-d}{w} + \frac{C}{R} \right) \cdot \frac{1}{\rho_{\text{matrix}}}$$

The surrounding layer (mean radius  $\bar{R}$ ) can thus be taken into account simply by a modified matrix resistivity.

Let us now assume, that no transport current  $I_T$  flows through the conductor. As the current density  $J_t$  within the filament bundle in the composite is homogeneous, there can be no net induced currents along the inner filaments.

All transverse currents must be collected by the filaments of the outer layer only. If there are  $N$  filaments in the outer layer of diameter  $D$ , the induced current  $I_F$  through each filament is:

$$\frac{dI_F}{dZ} = \pm \frac{2\pi}{l_p} \cdot \frac{dI_F}{d\varphi_p} = \frac{2\pi}{N} \cdot J_t \cdot \frac{D}{2} \cdot \sin(\varphi_p)$$

or:

$$I_F(\varphi_p) = \pm \int_0^{\varphi_p} \frac{dI_F}{d\varphi_p} \cdot d\varphi_p = \pm \frac{\pi}{N} \cdot J_t \cdot \frac{l_p}{2\pi} D \cos(\varphi_p) \quad (1.45)$$

The  $\cos(\varphi_p)$  distribution of the induced currents generates a homogeneous self field  $B_e$  in the direction of the field  $B_{\text{ext}}$ , justifying the assumption of homogeneous  $B$  over the conductor.

$$B_e = \frac{1}{2\mu_0} \cdot J_S = \frac{\mu_0}{2} I_F(0) \frac{N}{\pi D}$$

$$B_e = \pm \mu_0 \cdot \frac{J_t}{2} \cdot \frac{l_p}{2\pi} = \frac{\mu_0}{2} \left( \frac{l_p}{2\pi} \right)^2 \cdot \frac{1}{\bar{\rho}_c} \cdot (B_{\text{ext}} + B_e) \quad (1.46)$$

The azimuthal component of  $I_F(\varphi_p)$  produces a further component

of  $B$  in the direction of the conductor axis. For  $l_p \gg D$  this component can be neglected. The negative sign in Eq. (1.46) reflects the fact, that the induced currents counteract the change of the external field.

If  $\dot{B}$  is expressed by the change in transverse current density  $\dot{J}_t$ , one obtains the equation:

$$\frac{dJ_t}{dt} + \frac{2}{\mu_0} \left(\frac{2\pi}{l_p}\right)^2 \cdot \bar{S}_c \cdot J_t = \pm 2 \dot{B}_{ext} \left(\frac{2\pi}{\mu_0 l_p}\right) \quad (1.47)$$

The homogeneous solution of Eq. (1.47) yields, after a sudden change in  $B_{ext}$  occurs, an exponential decay for  $J_t$ :

$$J_t(t) = J_t(0) \cdot e^{-t/\tau} \quad (1.48)$$

Where the time constant  $\tau$ , is given by

$$\tau = \frac{\mu_0}{2} \left(\frac{l_p}{2\pi}\right)^2 \frac{1}{\bar{S}_c} \quad (1.49)$$

$\tau$  can be understood as the ratio of the inductivity of the filament loops and the matrix resistance. Fig. (1.10) illustrates for a triangular pulsed external field the transverse current  $J_t$  as well as the induced current  $I_F$  through the filaments, and the field  $B_e$  for two limiting cases of  $\tau \ll t_0/2$  and  $\tau \gg t_0/2$  with  $t_0$  denoting the pulse length. With increasing ratio of  $\tau/t_0$  the variation of the external field in the conductor is shielded more and more by the induced currents in the filaments. For  $\tau \ll t_0/2$  the losses in the matrix are modified only slightly by the transient phenomena.

The current carrying capacity of the filament is limited by the critical current  $I_c$ . Beyond this value flux crosses the outer layer of filaments. Energy is dissipated, leading to a longitudinal voltage drop. The next inner layer takes over the

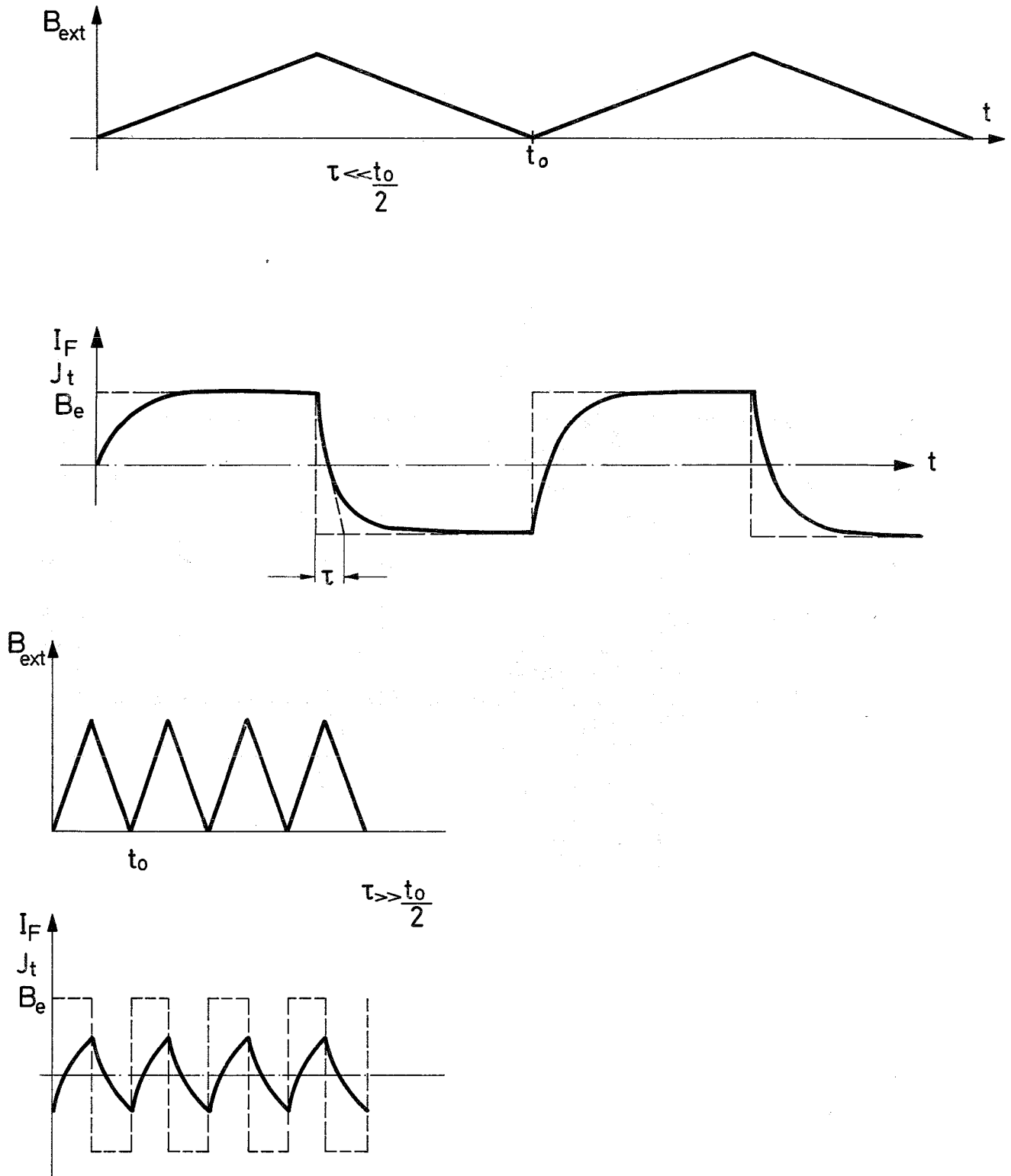


Fig.1.10

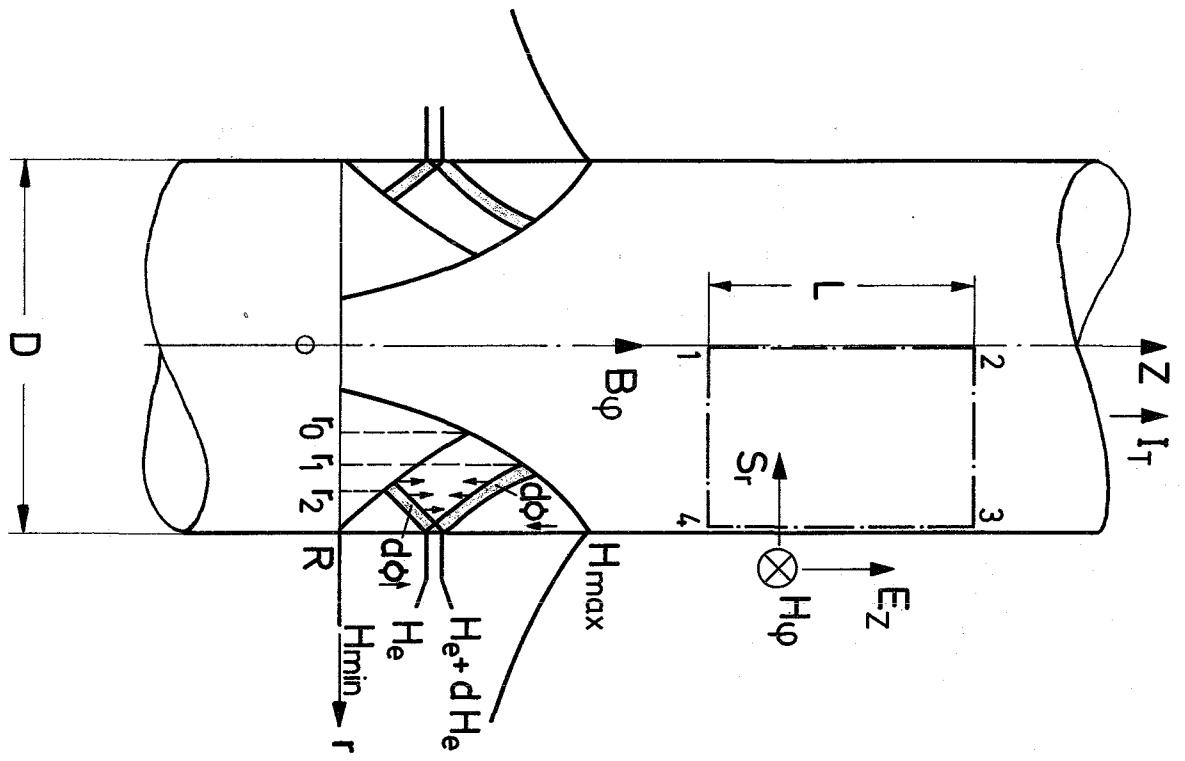


Fig. 1.11

excessive part of the shielding currents and leads to a partial coupling between filaments. By equating the induced screening current  $I_F$  ( $\varphi_p = 0$ ) from Eq. (1.45), with the critical current  $I_c$  for a single filament, assuming no transport current is flowing, we get a relation between field rise and the "critical twist length"  $l_c$ .

$$I_{F,\max} = I_c = \frac{1}{\bar{g}_c} \cdot \left(\frac{l_c}{2\pi}\right)^2 \cdot \frac{\pi D}{N} \cdot \dot{B} \quad (1.50)$$

The critical twist length  $l_c$  is expressed for  $\dot{B} \approx \dot{B}_{\text{ext}}$ , i.e. for  $\tau \ll t_0$  by:

$$l_c^2 = (2\pi)^2 \bar{g}_c I_c \cdot \frac{N}{\pi D} \cdot \frac{1}{|\dot{B}_{\text{ext}}|} \quad (1.51)$$

This equation is different by the numerical factor  $(\pi^3/32)^{1/2}$  from the expression MORGAN <sup>7)</sup> has obtained for a two filament conductor model (TV-cable).

For a sinusoidally varying field expressed by  $B_{\text{ext}} = \bar{B}_{\text{ext}} + \tilde{B}_{\text{ext}} \cdot \exp(j\omega t)$ , we consider only the variable part, and get from Eq. (1.47)

$$J_t = \frac{2}{\mu_0 l_p} \cdot \tilde{B}_{\text{ext}} \cdot \left(1 + \frac{1}{j\omega\tau}\right)^{-1}$$

and obtain the losses per unit volume from:

$$p_e = \frac{J_t^2}{2} \cdot \bar{g}_c = \frac{(\tilde{B}_{\text{ext}})^2}{4\mu_0} \left(1 + \frac{1}{\omega^2\tau^2}\right)^{-2} \quad (\text{W}) \quad (1.52)$$

For  $\omega \ll \frac{1}{\tau}$  (low frequencies),  $p_e$  is proportional to  $\omega^2$ .

This is different from the frequency dependence of hysteretic losses, which are proportional to  $\omega$ !

As  $p_e$  is also proportional to  $\tau$ , high resistivity matrix materials and short twist pitch are recommended in contrary to the dynamic stability criterion, which requires low electrical resistivity materials.

With increasing frequency, eddy current losses approach the value of  $p_e = (\tilde{B}_{ext})^2 / 4\mu_0\tau$ . The field variation within the composite decreases with increasing frequency due to shielding currents.

From  $B_{ext} = \bar{B}_{ext} + \tilde{B}_{ext} \exp(j\omega t)$ , and  $B_e = B - B_{ext} = -\tau \cdot \dot{\tilde{B}}$ , we get for the alternating part of the field seen by the filaments

$$\tilde{B} = \tilde{B}_{ext} \cdot e^{j\omega t} (1+j\omega\tau)^{-1}$$

This part induces the common hysteretic losses due to flux movements in the superconductor. These losses depend only on the maximum and minimum field values.

The inner filaments of a bundle which are not forced to carry screening currents, see only the shielded field, and the dissipated energy per cycle decreases with  $1/|1+j\omega\tau|$ . This means that the average hysteretic loss rate approaches a constant value with increasing frequencies. This conclusion may be of interest for industrial (i.e. 50Hz) applications.

Qualitative confirmation of this effect was obtained by McInturff<sup>8)</sup> for the similar case of transposed braids with a metallic insulation<sup>+</sup>. At a field change of  $\dot{B} \gtrsim 4$  T/sec, the dissipation rate approached a constant value.

The above model is applicable to metallic insulated cables where multifilament conductors are simply twisted. Transposed cables and braids will show a more or less complicated internal eddy current distribution pattern depending on the manufacturing

---

<sup>+</sup> Metallic insulation refers to as solder of high electrical resistivity such as Sn-Ag or Sn-In alloy or others.

procedure. For this case the model developed here will be no longer in quantitative agreement with the experimental data.

### 1.12 Self field losses

It may be pointed out, that in the treatment of losses up to now the effect of field inhomogeneities on the conductor was not considered. Specifically the self field effect due to transport currents in the wire has the same origin as the skin effect in the normal conductor and tends to exclude current density changes in the interior of the wire. This effect is not compensated by simple twisting, but by transposition of filaments.

Flux changes induced by the self fields in a superconductor lead to movement of fluxoids within the superconductor and thus to dissipative losses. These losses are of electromagnetic nature and may be obtained by integrating the Poynting vector  $\vec{S} = (\vec{E} \times \vec{H})$  over the conductor surface. The irreversible part of this energy, integrated over a cycle is dissipated as heat.

The component  $S_r$  of the Poynting vector, perpendicular to the conductor surface is obtained from the azimuthal component of the self field  $B_\varphi(R) = \mu_0 I / 2\pi R$  and the axial component of the electric field  $E_z$  at the conductor surface, when the flux penetrates the surface.

From Fig. (1.8) we obtain the voltage for a closed loop C:

$$V = \oint_C \vec{E} \cdot d\vec{s} = - \dot{\Phi} = - \int \dot{B}(r) dr \cdot L = E_z \cdot L \quad (1.53)$$

The electric field is zero on the conductor axis  $\overline{1-2}$  and has no contribution to  $\overline{2-3}$  and  $\overline{4-1}$ . The electric field  $E_z$  is directed such to exclude current changes from the interior of the conductor. Only if the critical current density is exceeded in the superconductor, an associated longitudinal voltage drop is generated. The self field due to the transport current can penetrate further into the composite conductor.

Evidently, the critical state model, developed for a supercon-

ductor located in an external field, is also valid for the self field penetration produced by a transport current.

The model is still valid for a multifilament conductor, if the integration path  $\overline{1-2}$  and  $\overline{3-4}$  of Fig.(1.11) are chosen along the filaments. An external field can enter the matrix without flux flow (if  $l_p \ll l_c$ ) whereas for the self field the same conductor behaves as a compact filament.<sup>+</sup>)

In magnets the external field is much higher than the self field of the conductor. Thus  $J_c$  is the same across the conductor and the Bean-model, modified for a cylindrical geometry can be applied. At a peak current  $I_{max}$ , the critical state current density  $J=J_c$  penetrates the conductor up to a radius  $r=r_o$ . This current is given by  $I_{max} = \bar{J}_c \pi (R^2 - r_o^2)$ , where  $R$  denotes the radius of the composite conductor. The associated self field  $H_\varphi(r)$  is given by  $\text{curl } H = J$ , which in the cylindrical geometry is expressed by

$$\frac{dH_\varphi}{dr} + \frac{H_\varphi}{r} = J_z \quad (1.54)$$

and has the solution:

$$H_\varphi(r) = \pm \frac{rJ_c}{2} \pm \frac{R}{r} \left( H_e - \frac{\bar{J}_c R}{2} \right) \quad (1.55)$$

The ( $\pm$ ) sign depends on the sign of  $J_z = \pm J_c$ . The field  $H_e$  denotes the self field  $H_\varphi(R)$  at the conductor surface. During current cycling in the range between  $I_{min}$  and  $I_{max}$ , self field patterns as shown in Fig. (1.12) are obtained. The nonlinear field  $H_\varphi(r)$  is the field generated of concentric tubes each having a uniform current density  $\pm \bar{J}_c$ .

---

<sup>+</sup>For simplification the filamentary structure of the conductor is replaced by a single conductor having a mean current density  $\bar{J}_c$ .

The change of the field  $B_{\varphi}(r)$  in the conductor is linked to the variation of the self field  $H_e = I/2\pi R$  by:

$$\frac{dB_{\varphi}(r)}{dt} = \mu_0 \frac{dH(r)}{dH_e} \cdot \frac{dH_e}{dt} = \mu_0 \cdot \frac{R}{r} \cdot \frac{dH_e}{dt} \quad (1.56)$$

The dissipative part of  $\vec{S}$  is obtained from the difference of  $\dot{\phi}$ , if the transport current  $I_T$  is raised (field energy is entering the probe) and then reduced (part of the field energy leaves the probe) as illustrated in Fig. (1.11).

Thus from  $E_z = V/L$ , we obtain:

$$\begin{aligned} E_z^{\uparrow} - E_z^{\downarrow} &= -\mu_0 \left[ \int_{r_2}^R \frac{R}{r} dr - \int_{r_1}^R \frac{R}{r} dr \right] \left| \frac{dH_e}{dt} \right| \\ &= -\mu_0 \left| \frac{dH_e}{dt} \right| \cdot R \cdot \ln \left( \frac{r_2}{r_1} \right) \end{aligned} \quad (1.57)$$

The values of  $r_1$  and  $r_2$  are obtained from the relations:

$$H(r_1) = \frac{r_1}{z} \bar{J}_c + \frac{R}{r_1} \left( H_{\max} - \frac{\bar{J}_c R}{z} \right) = -\frac{r_1}{z} \bar{I}_c + \frac{R}{r_1} \left( H_e + \frac{\bar{J}_c R}{z} \right)$$

from which we calculate:

$$r_1 = R \left[ 1 - \frac{H_{\max} - H_e}{\bar{J}_c R} \right]^{1/2} \quad (1.58)$$

and

$$r_2 = R \left[ 1 - \frac{H_e - H_{\min}}{\bar{J}_c R} \right]^{1/2} \quad (1.59)$$

Self field losses per cycle can be calculated for a conductor with a surface area of  $2\pi RL$  by integrating  $(E^{\uparrow} - E^{\downarrow}) \cdot H_e$ , over half a cycle.

To simplify calculations we have assumed that  $J_c$  is independent of the field:

$$W_{sf} = 2\pi R^2 L \int_0^{t_0/2} H_e \cdot (E_z \uparrow - E_z \downarrow) dt$$

$$= \pi R^2 L \mu_0 \int_{H_{min}}^{H_{max}} H_e \left[ \ln \left( 1 - \frac{H_{max} - H_e}{J_c R} \right) - \ln \left( 1 - \frac{H_e - H_{min}}{J_c R} \right) \right] dH_e$$

which after integration is rearranged to the form:

$$W_{sf} = \pi \bar{J}_c^2 R^4 L \mu_0 \left\{ \left( 1 - \frac{H_{max} - H_{min}}{J_c R} \right) \cdot \left[ \ln \left( 1 - \frac{H_{max} - H_{min}}{J_c R} \right) + \frac{H_{max} - H_{min}}{J_c R} \right] + \frac{1}{2} \left( \frac{H_{max} - H_{min}}{J_c R} \right)^2 \right\} \quad (1.60)$$

Modifying this equation for transport currents instead, one uses  $I_c = \pi R^2 J_c$  the critical short sample current, and introduces the transport current difference  $\Delta I$ . This is the change in current from the lowest to the peak value expressed by:

$$\frac{H_{max} - H_{min}}{J_c R} = \frac{\Delta I}{2\pi \bar{J}_c R^2} = \frac{\Delta I}{2I_c}$$

For a transport current cycled between the values  $+I_0$  and  $-I_0$ , Eq. (1.60) is identical to the expression derived by Hancox<sup>9</sup> for a cylindrical compact superconductor without external field.

The logarithmic term in Eq. (1.60) is expanded in a power series, and one obtains:

$$W_{sf} = I_c^2 L \frac{\mu_0}{\pi} \left[ \frac{1}{2 \cdot 3} \left( \frac{\Delta I}{2I_c} \right)^3 + \frac{1}{3 \cdot 4} \left( \frac{\Delta I}{2I_c} \right)^4 + \dots \right] \quad (1.61)$$

or:

$$W_{sf} = (\Delta I)^2 L \frac{\mu_0}{4\pi} \cdot \left[ \frac{1}{2 \cdot 3} \left( \frac{\Delta I}{2I_c} \right) + \frac{1}{3 \cdot 4} \left( \frac{\Delta I}{2I_c} \right)^2 + \dots \right] \quad (1.62)$$

As  $(\Delta I) \cdot L$ , (total current multiplied by the length of a strand) is constant for a coil of a given geometry, the self field losses are proportional to  $\Delta I$  and thus to the square of the diameter  $D$  of the composite conductor.

For  $D \rightarrow \infty$  (as for a slab), the only remaining term in Eq. (1.60) is:

$$W_{sf} = \mu_0 \cdot \frac{\pi RL}{6J_c} \cdot (H_{\max} - H_{\min})^3 \quad (1.63)$$

which is essentially the expression Bean obtained for hysteretic losses in a slab with a surface area of  $2\pi RL$  located in an external field parallel to the surface of the slab and cycled between the field values  $H_{\min}$  and  $H_{\max}$ .

### 1.13 Contribution of external fields

In the above calculation we had omitted the influence of a superposed external field in addition to the self field in the Poynting vector at the conductor surface, which will now be rectified.

The axial field component  $(B_{\text{ext}})_z$  is parallel to  $E_z$  and does not contribute to  $W_{sf}$ . The transverse field component can be expressed in the form of multipoles:

$$\begin{pmatrix} B_{\text{ext},\varphi} \\ B_{\text{ext},r} \end{pmatrix} = \sum_{n=1}^{\infty} B_{\text{ext},n} \cdot r^{n-1} \cdot \begin{pmatrix} \cos(n\varphi) \\ \sin(n\varphi) \end{pmatrix} \quad (1.64)$$

All terms of the series with  $n > 1$  describe higher field multipoles. As mentioned, hysteretic and eddy current losses can be expressed by a Poynting vector at the surface of the conductor due to the electric field  $E_{z,\text{ext}}(\varphi)$ , for which a similar harmonic expansion as for  $B_{\text{ext},\varphi}$  is valid with  $n \geq 1$ .

Combined with the self fields  $E_{o,z}, H_{o,\varphi}$  (which are independent of  $\varphi$  in the cylindrical case), the Poynting vector can be expressed by:

$$S_{\text{tot}} = (E_{\text{ext},z} + E_{o,z}) \cdot (H_{\text{ext},\varphi} + H_{o,\varphi})$$

$S_{\text{tot}}$  integrated over the conductor surface gives only the contribution of the external field and of the self field as evaluated above, while the mixed terms yield no contribution. This means that the loss sources can be treated independently even in the case of a nonuniform external field.

#### 1.14 Discussion:

The equations for self field losses were derived, assuming  $\bar{J}_c$  is constant. If  $\bar{J}_c$  changes with the applied field (e.g. due to the self field of a coil, where  $B_{\text{ext}} \propto (I)$ , Eq.(1.62) must be corrected by using  $\bar{J}_c (B_{\text{ext}}(I))$ . The two integration boundaries  $r_1$  and  $r_2$  must also be modified. Analytical integration over one cycle is no longer possible. Self field losses in a coil can be approximated if one uses a  $\bar{J}_c$  value at an average field over the entire coil and a complete cycle which is about a quarter of the aperture peak field.

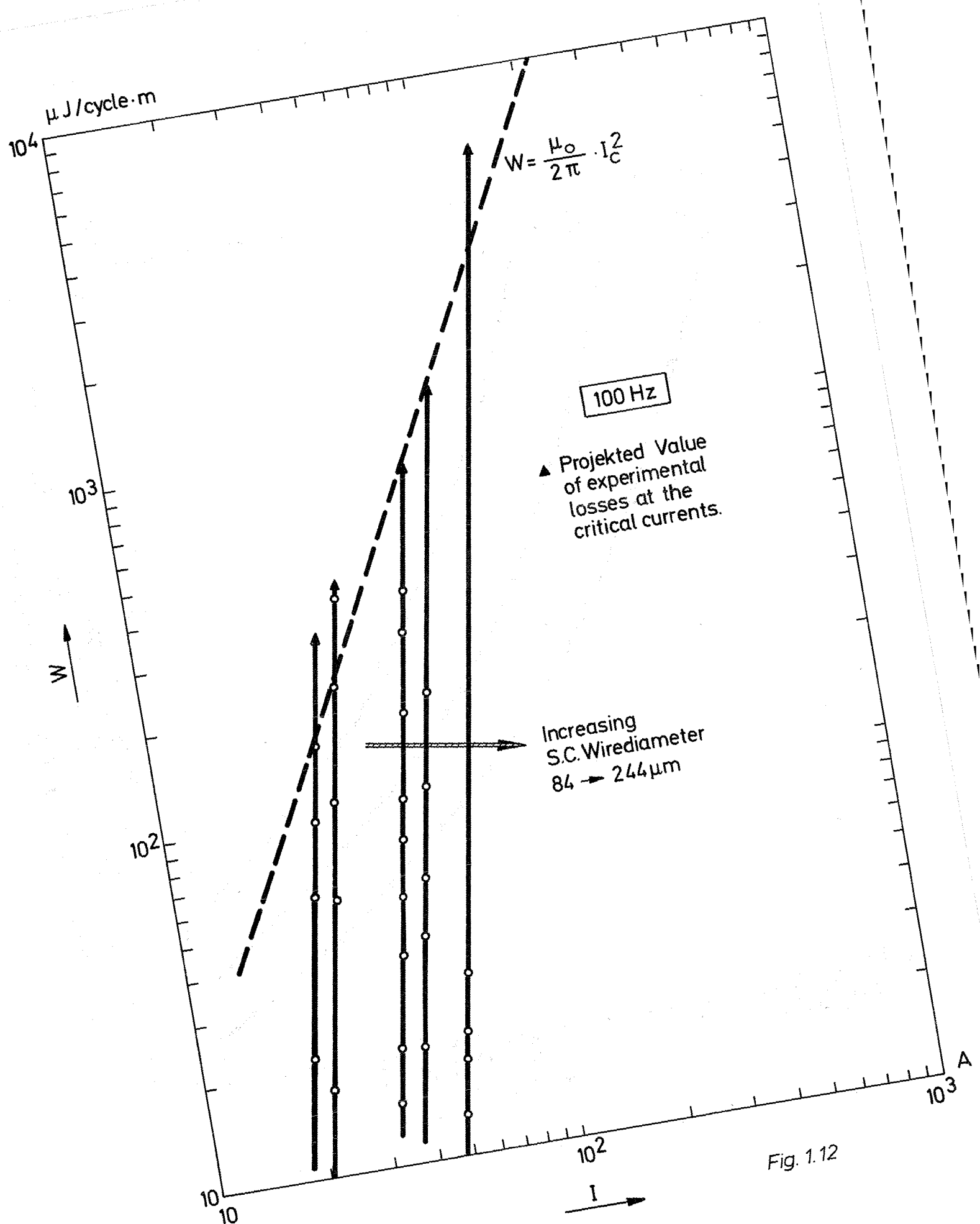
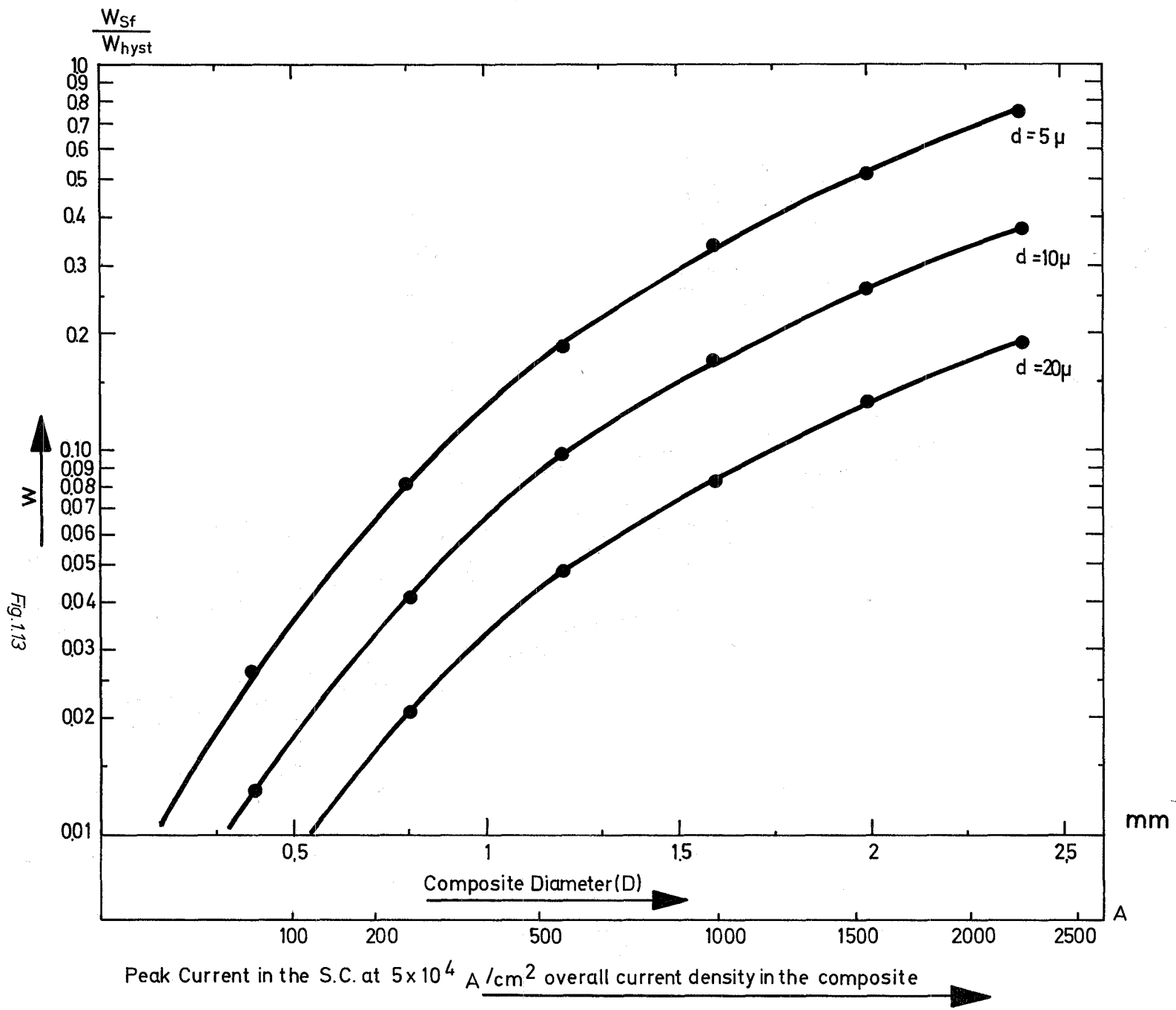


Fig. 1.12



For a zero external field, losses were measured for a changing transport current in the range of  $-I_o \rightarrow 0 \rightarrow +I_o$  for 5 samples as shown in Fig. (1.12). Losses for  $I_o = I_c$  are denoted by triangles. The broken line is calculated from Eq. (1.62) for  $\Delta I = 2I_c$  which yields per unit conductor length the relation:

$$W_{sf,max} = \frac{\mu_o}{2\pi} I_c^2 \quad (1.65)$$

### 1.15 Comparison between self-field and hysteretic Losses

It was shown that the hysteretic losses are proportional to  $d$ , the diameter of the individual filament and the self field losses proportional to the square of the diameter  $D$  of the strand or composite conductor. For practically all superconducting magnets  $\frac{\Delta I}{2I_c} \ll 1$ , thus we may neglect all higher terms in Eq. (1.62). Assuming a constant critical current density as in the case of  $W_{sf}$ , we may write for the hysteretic losses:

$$W_{hl} = \mu_o J_c \frac{d}{2} V \Delta H_{ext}$$

with  $V$  the conductor volume.  $\Delta H_{ext}$  is the maximum range of the changing external field in one cycle.

The self field losses are given approximately by:

$$W_{sf} = \mu_o \pi \frac{D^4 \bar{J}_c^2 L}{4 \cdot 192} \left(\frac{\Delta I}{I_c}\right)^3 = \mu_o \frac{D^2 \bar{J}_c V}{192} \left(\frac{\Delta I}{I_c}\right)^3 \quad (1.66)$$

Thus:

$$\frac{W_{sf}}{W_{hl}} = \frac{D^2}{d} \frac{\bar{J}_c}{96} \frac{\left(\frac{\Delta I}{I_c}\right)^3}{\Delta H_{ext}} \quad (1.67)$$

For a magnet with  $\Delta H_{\text{ext}} = 20 \times 10^3 \text{ Acm}^{-1}$ ,  $J_c = 10^5 \text{ Acm}^{-2}$ , ( $J_c(H)$  at one quarter of the peak field value) and  $\Delta I/I_c = 0.5$  one obtains

$$\frac{W_{\text{sf}}}{W_{\text{hl}}} \approx 0.65 \frac{D^2}{d}$$

where  $D$  is expressed in (mm) and  $d$  in ( $\mu\text{m}$ )!

Fig. (1.13) illustrates this relation for a pulse magnet with a 5T peak field at  $5 \times 10^4 \text{ Acm}^{-2}$  overall current density.

#### 1.16 Modification of the hysteretic losses, if the transport current is not zero.

In section (1.6) it was shown, that the hysteretic losses in a superconducting slab, carrying a transport current  $I_T$ , is increased by the factor,  $[1 + (\frac{I_T}{I_c})^2]$ . Nearly the same factor is expected for cylindrical conductors.

As shown in the preceding chapters, according to Bean's critical state model only the outer filaments in the penetration region carry the transport current. This is particularly true in the low field region of the coil due to the high current carrying capacity of type II materials at low fields.

In addition even in the penetration region,  $r_0 - R$  (see Fig. (1.11)), the part  $r_0 - r_1$ , respectively  $r_0 - r_2$ , of filaments is not in its critical state condition except near the current maximum. The reason is that the individual current per filament, given by its critical value at the field maximum is conserved at low field levels, where as  $I_c$  increases, such that the correction factor  $1 + (\frac{I_T}{I_c})^2$  is zero or very small for a large portion of filaments during most time of the field cycle. The overall correction, which would be difficult to evaluate is expected to be small and can be neglected in comparison with other error sources such as in  $J_c(H)$ , filament diameter, matrix resistivity, average field over the coil etc.

## 2. Additional effects in twisted multifilament conductors

### 2.1 Axial diffusion of the self field

As shown, changes of the transport current can be accepted by the inner filament circles only, if the flux density  $B$  produced by the self field changes in the space between adjacent filaments. This requires that

$$\oint \vec{E} d\vec{S} = - \dot{\phi} \neq 0 ;$$

as shown, a voltage appears at the outer filament circle only if the current exceeds the critical  $J_c$  value and the vortices start to move.

Even if the critical current is not exceeded in the outer filament circles, a voltage can appear across matrix material as a result of currents flowing between filaments.

In the following the derivation of the diffusion equation of the self field  $B_\varphi(r)$  inside a composite multifilament conductor is given. Here the twist induced current density in the noncritical inner part of the conductor is neglected temporarily but may be added to the result as a first approximation. The conclusion of this calculation may give one possible explanation of the degradation phenomena observed in long conductors compared to short sample values:

As shown, the self field

$$B_\varphi(r) = \mu_0 \frac{I(r)}{2\pi r}$$

describes also the acceptance of current by the inner filament circles, where  $I(r)$  is the portion of the transport current, which (in case of cylindrical geometry) flows within a cylinder of radius  $r$ .

We consider an area  $dF = dz \cdot \Delta r$  between two filament circles, Fig. (2.1), of radii  $r_1$  and  $r_1 + \Delta r = r_2$ . The paths 1-2 and 3-4 are located in the electrical center of the filaments, to avoid potential differences over these passages.

The flux  $d\phi$  through  $dF$  depends on the current  $I(r_1, z)$  flowing through filaments located within the cylinder with a radius  $r_1$ :

$$d\phi = \mu_0 dz \Delta r \cdot \frac{I(r, z)}{2\pi r} \quad (2.1)$$

Eq. (2.1) is true only if  $\Delta r \ll r_1, r_2$ .

The induced voltages are given by:

$$\begin{aligned} U_{14} - U_{23} &= \frac{\partial U}{\partial z} dz = - \dot{d\phi} \\ &= - \mu_0 \cdot \frac{1dz}{2\pi r} \Delta r \frac{dI(r, z)}{dt} dz \end{aligned} \quad (2.2)$$

The voltage  $U(z)$  between filament circles generates radial cross currents flowing through the matrix, i.e. the transport current must be redistributed in the  $z$  coordinate between the outer ( $r \geq r_1$ ) and inner ( $r \leq r_1$ ) filaments.

An external field (assumed homogeneous) produces a flux  $d\phi$ , but the additional induced eddy currents are only small, if the twist pitch is short enough and yields a sinewave modulation of the current along the filament (see chapter (1.10)).

If the electrical conductivity of the matrix material is  $\sigma$ , the radial current density in the matrix can be given by:

$$J_r(r, z) = \frac{U(z) \cdot \sigma}{\Delta r} \quad (2.3)$$

With  $\Delta r$  an averaged distance between filaments.

Combining Eq. (2.2) and Eq. (2.4) we obtain the differential equation for the current  $I(r)$ :

$$\begin{aligned} \frac{\partial^2 I(r,z)}{\partial z^2} &= 2\pi r \frac{\sigma}{\Delta r} \cdot \frac{\partial U}{\partial z} \\ &= -\mu_0 \frac{\Delta r}{\Delta r} \cdot \sigma \frac{dI(r,z)}{dt} \end{aligned} \quad (2.5)$$

The self field penetration in the filament bundle and with it, the current distribution (assuming there is no longitudinal voltage drop along the superconductor, which is true for  $J < J_c$ ), can so be accomplished axially according to a diffusion equation with a diffusion constant:

$$D_m = \frac{\overline{\Delta r}}{\mu_0 \sigma \Delta r} \approx \frac{1}{\mu_0 \sigma}$$

Solution of  $I(r,z,t)$ :

- 1) for a conductor extended infinitely in z-direction carrying a transport current there is no z-dependent solution of the current  $I(r,z,t)$ :

$$\frac{\partial I(r,z,t)}{\partial z} = 0$$

Self field flux and transport current can only penetrate radially through the flux flow mechanism.

- 2) The multifilament conductor is connected at one end ( $z=0$ ) to a normal metal e.g. the superconducting coil winding to the current lead.

The small change  $\Delta I$  of the total transport current  $I_{tot} = I(R,z,t)$  independent of already flowing equilibrium currents  $I_0(r)$  shall at  $t=0$  be according to a step function:

$$I(R,0,t) = I_0(r) + \Delta I \theta(t)$$

$$\theta = \begin{cases} 0 & \text{for } t < 0 \\ 1 & \text{for } t > 0 \end{cases}$$

If  $I < I_c$ , the filaments at the outer circle will carry at  $t = 0$  the entire current  $\Delta I$ . The current in the inner filaments are forced radially outwards through the matrix by means of induced anticurrents at  $z \geq 0$ , as discussed in (1.12)

As illustrated in Fig. (2.2) the initial situation is developing according to the solution of Eq. (2.5) with the described boundary conditions at  $t = 0$ :

$$I(r,z,t) - I_0(r) = (I(r,0,0) - I_0(r)) \left[ 1 - \frac{2}{\sqrt{\pi}} \int_0^{\xi} e^{-u^2} du \right] \quad (2.6)$$

where

$$\xi = \frac{z}{2 D_m t} = \frac{z}{2} \sqrt{\frac{\mu_0 \sigma}{t}}$$

In the case of a nonideal joint (normal metal-superconductor) the current will flow even in the normal metal as illustrated in Fig. (2.2) for  $z < 0$ .

In reality the transient zone is not as well defined as assumed for the idealized case, but the general behaviour will be the same:

From the ends of the composite a zone of non-stationary current distribution penetrates the conductor which is no longer determined by the critical state model for the self field, but tends for  $t \rightarrow \infty$  to equilibrium current sharing between filaments as given by the transition resistance between the current lead (normal conductor) and each single filament.

In a copper matrix with  $\frac{\rho_{300}}{\rho_{4.2}} = 100$ , the magnetic diffusion constant has a value of

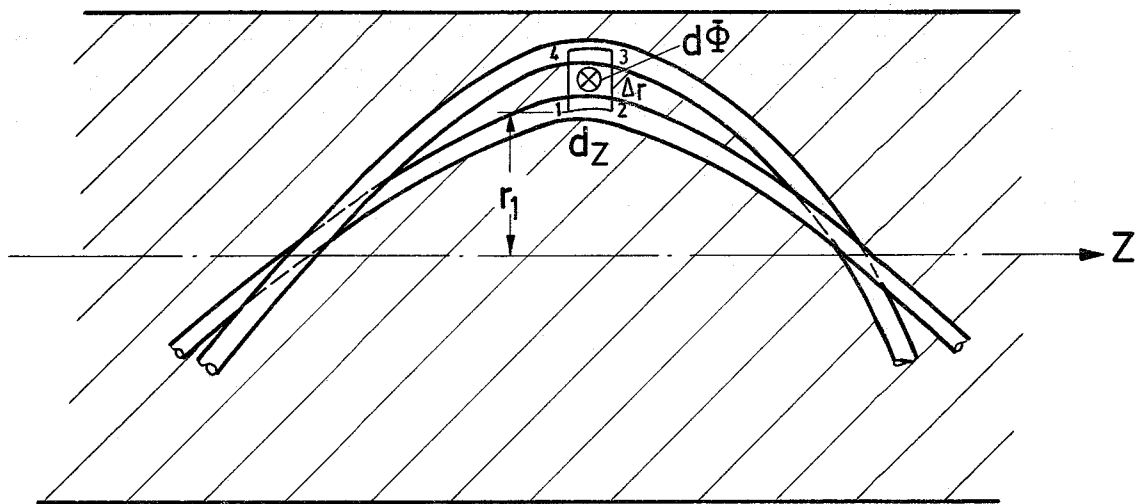


Fig. 21

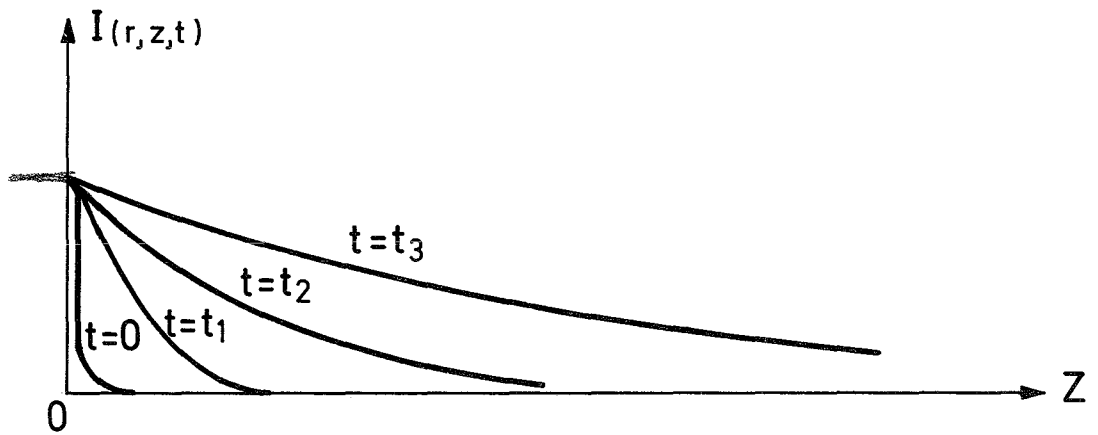
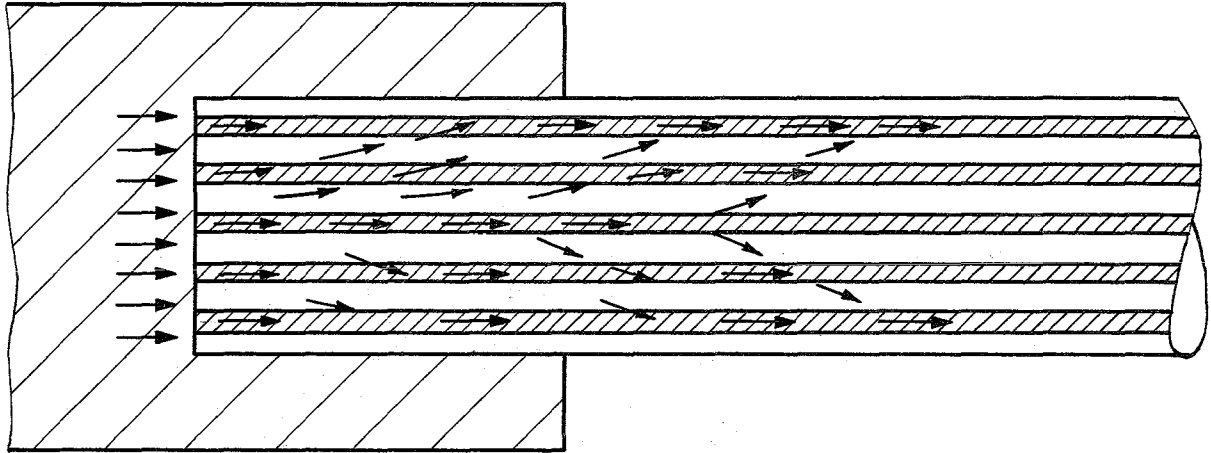


Fig. 2.2

$$D_m = \frac{1}{0.4 \cdot 10^{-8} \cdot 56 \cdot 10^4 \cdot 100} = 1.42 \text{ cm}^2 \text{ sec}^{-1}$$

In Nb-Ti composite conductors a high resistive Cu-Ti interlayer is present between filaments and copper matrix, which does decrease the effective matrix conductivity  $\sigma$  and thus increases  $D_m$  considerably.

3) A similar current profile is to be expected as for (2), if a disturbance occurs over a short section of a long conductor. We assume that a flux jump occurs in the outer filament circles and with it a longitudinal voltage is generated. A part of the transport current will be transferred to the next inner filament circle through the matrix. The corresponding self field penetrates through the resistive part into the space between filaments, from where it is propagated axially to both sides according to the diffusion equation, even when the overloaded filaments carry again stationary currents.

As the superconducting properties are not completely homogeneous along a composite conductor, it must be assumed, that changes in transport current and the related self field distribution across the outer filament circles by flux flow or flux jumps usually occur in those "hot spots" and propagate from here on along the conductor.

With respect to instabilities this situation is worse than at the previous assumption of an uniformly penetrating front of current and self field, as the heating in the overcritical filaments and the current carrying matrix is concentrated around these "hot spots" in this dynamic model. The total self field flux and thus the dissipated heat which must penetrate for a certain  $\Delta I_T$  to be overtaken by an inner filament circle, depends on the velocity. The penetrating self field gives the amount of current transferred to the inner part of the conductor and increases until the disturbed filaments recover again. If the heat is removed insufficiently, the heated spot expands and a quench occurs due to "self field instability" even when the short sample current of the conductor is not reached.

Low magnetic diffusivity  $D_m$ , a high thermal conductivity of the matrix and a good bond between matrix and filaments, reduces energy dissipation and favours recovery without quench. In short samples self fields can penetrate through the ends towards the middle of the wire in a reasonable time and a nearly uniform current density across the conductor is obtained after a few diffusion time constants, related to the half length.

This effect may give a possible explanation for the often observed degradation of the critical current in coils compared to  $I_c$ -values measured in short samples.

We apply a sudden current change  $\Delta I_T$  at  $t=0$  to a conductor of length  $2L$ . The corresponding current value  $\Delta I(r,L)$  in the middle of the conductor attains 50% of its final value at a diffusion time for which

$$1 - \frac{2}{\sqrt{\pi}} \int_0^{\xi} e^{-u^2} du = 1 - \phi \left( \frac{L}{2\sqrt{D_m T_{SS}}} \right) = 0.25 \quad (2.7)$$

is valid. (Penetration from both ends).

The appropriate diffusion time for a short sample with  $2L = 10\text{cm}$ , and magnetic diffusivity  $D_m = 1.42 \text{ cm}^2 \text{ s}^{-1}$  is:

$$T_{SS} = 6.62 \text{ sec.}$$

a time which may be considered small compared to the current rise time during short sample measurements, giving the full current carrying property of the composite.

On the other hand, if 100 m of this wire are wound into a coil, the diffusion time, propotional to the length square, yields,

$$T_{LS} = 6.62 \cdot 10^6 \text{ sec}$$

In this case current penetration imposes self field flux flow and quenching may occur even if the single filament is still stable in the external field.

## 2.2 Extension of the self field model in twisted multifilament conductors

In cylindrical multifilament conductors with twisted filaments, the transport current flowing through a filament has a screw type path on a cylindrical surface of radius  $r$  and forms a pitch angle  $\phi_p$  with the conductor axis. We may write for the pitch angle:

$$\tan(\phi_p) = 2\pi r/l_p \quad (2.8)$$

with  $l_p$  the length of the twist pitch and  $r$  the distance to the conductor axis.

The transport current density has two components: An axial current density component  $J_T$ , and due to the twist an azimuthal component  $J_\phi$ . These two components are related to each other by:

$$J_\phi = J_T \tan(\phi_p) \quad (2.9)$$

$J_\phi$  produces an additional solenoidal self field within the conductor in axial direction.

This field couples the twisted filaments like a mutual inductance and thus produces a modification of the transport current distribution:

We denote the self field components by  $B_\phi(r)$  and  $B_z(r)$  in the conductor at a radius  $r$ ,  $I(r)$  is the axial component of the

transport current flowing within a cylinder of radius  $r \leq R$ ,  $B_z$  is generated only from the current  $(I_T - I(r))$  outside  $r$ . If  $I_T$  is the total transport current, then

$$B_z(r) = \mu_0 \frac{I_T - I(r)}{l_p} \quad (2.10)$$

$B_\varphi$  is generated only from  $I(r)$ :

$$B_\varphi(r) = \mu_0 \frac{I(r)}{2\pi r} \quad (2.11)$$

$I(r)$  is determined from the boundary condition, that no flux-changes due to the self field can occur through a plane passing through any two arbitrary filament axis.

This means that in a simplified model, in which the heterogeneous current pattern is smoothed out by averaged values, the resulting self field must be parallel to the filament and thus forms an angle  $\varphi_p$  with the conductor axis

$$\frac{\dot{B}_\varphi}{\dot{B}_z} = \frac{\dot{I}(r)}{2\pi r} \cdot \frac{l_p}{\dot{I}_T - \dot{I}(r)} = \tan(\varphi_p) = \frac{2\pi r}{l_p} \quad (2.12)$$

From which we calculate  $\dot{I}(r)$ :

$$\dot{I}(r) = \frac{\dot{I}_T}{1 + \left(\frac{l_p}{2\pi r}\right)^2} = \frac{\dot{I}_T}{1 + \cotan^2(\varphi_p)} \quad (2.13)$$

Integrating  $\dot{I}(r)$  with respect to time gives the value of  $I(r,t)$ :

$$I(r,t) = \frac{I_T(t) - I_T(0)}{1 + \cotan^2(\varphi_p)} + I(r,0) \quad (2.14)$$

The magnetic coupling due to currents flowing through twisted filaments forces the filaments at the inner conductor parts to overtake a part of transport current without the condition that accompanying self field has passed across the outer filaments by the flux flow mechanism<sup>11)</sup>.

Clearly in the calculated self field formula the inserted transport current  $\Delta I$  is reduced by this fraction, which penetrates the conductor without energy dissipation.

Eq. (2.14) has been derived using the condition that the electrical field along the filaments during the change of the transport current is negligible. This is true only in the conductor region, where the critical current in the filaments is not exceeded, i.e. in the interior cylindrical portion of the conductor, while in the outer region of self field penetration the filaments carry the critical current.

The average current density is thus given by:

$$\bar{J}(r) = \frac{1}{2\pi r} \cdot \frac{dI(r)}{dr} = I_T \cdot \frac{4\pi l_p^2}{(4\pi^2 r^2 + l_p^2)^2} \quad (2.15)$$

(with  $I(r,0) = I_T(0) = 0$ ).

The self field  $B(r)$  and the current density  $J(r)$  are illustrated for maximum and minimum value of  $I_T = I_{\max}$  and  $I_T = I_{\min} = 0$  in Fig. (2.3).

### 3. Eddy current losses in metallic parts

#### 3.1 Iron losses in the flux return path:

For completion one has also to consider losses in metallic coil reinforcements, in the metallic helium container and other metallic parts surrounding the coil. In beam transport magnets the iron shell is also placed within the helium container and must be cooled by the helium. Eddy current losses in all metallic parts can be calculated in analogy to section (1.11). Iron losses (without end effects) are given by:

$$p_{\text{core}} = G_{\text{Fe}} (\sigma_e f^2 B_m^2 + \sigma_h f B_m^h) \quad (3.1)$$

$\sigma_h$  and  $\sigma_e$ , are material constants due to hysteretic and eddy current effects in iron. The exponent  $h$  varies in the range of 1.6-2,  $G_{\text{Fe}}$  is the weight of the laminated core,  $f$  the frequency of the pulsed field.

Core endlosses can be reduced either by shaping the core end-section (Rogowski shapes) or by extending the iron yoke about 2 times aperture diameter over the coil ends.

### 4. Comparison of loss-calculation with experiments.

Comparison of results obtained from theoretical considerations and experimental investigation requires the exact knowledge of the location and distribution of superconducting filaments within a single strand and in the cable or braid, the physical properties of the matrix material, and the type of impregnation used (i.e. metallic, intermetallic or organic) in the cable. It is not possible, to introduce a simple universal theory which includes the effect of various components mentioned. Difficulties in manufacturing a.c. cables have lead to discrepancies between theory and experiments (broken filaments, interturn, shorts, etc.).

Published data on loss measurements<sup>8,12,13</sup>) agree reasonably well with theoretical calculations only in special cases. Generally due to lack of detailed information, experimental data on a.c. magnets do not fit theoretical predictions. Good agreement between theory and experiment is reported by laboratories in magnets, which they have build and all coil and conductor data are available. Conductors used so far in pulsed superconducting magnets are multistrand cables or braids, with each strand consisting of twisted fine superconducting filaments embedded in a two or one component normal metal matrix<sup>†</sup>. The strands are twisted or transposed and shaped to desired rectangular configurations. The individual strands are either insulated individually, or impregnated in a metallic or intermetallic insulator.

The size of the individual strand in a cable or braid needed for coil construction is determined by the type of conductor. In cables containing individually insulated strands, it is desired to use large size wires containing many superconducting filaments. Larger strand sizes have also the advantage of ease of cabling and compacting without wire breakage. These types of conductor have a higher packing factor (ratio of wire to insulation). The largest conductors manufactured so far have a compacted size of 0.5x0.5 cm and carry 5600 A at 4.5T, (RHEL).

Common shapes of conductors are 2000 A (at 5.0T) cables, having a cross-sectional area of  $(2.6 \times 2.1) \text{mm}^2$ , selected for the  $D_2$  dipole at Karlsruhe, the braid selected by Siemens has a cross-section of  $(5 \times 0.6) \text{mm}^2$  and carries  $\sim 1000$  A at 5T. Saclay chosen a 24 strand braid, with 0.4 mm strand diameters each braid having 1000 filaments. The conductor carries 1500 A at 6.7T.

---

<sup>†</sup>The one component matrix used in low resistivity copper (generally OFHC) or aluminum; two component matrix used is low resistivity copper and cupronickel.

The size of each strand selected for different braids or cables vary between 0.02-0.04 cm, but may exceed 0.1 cm diameter, as it was found that self field effects are quite small as shown in Eq. (1.62). However, the filaments should be decoupled in order to eliminate additional losses. Decoupling is achieved by adequate twisting and the use of cupronickel around individual filaments or clusters of filaments. Standard cables consist of a number of twisted strands. These cables have the disadvantage that concentric layers of strands within the cable are geometrically displaced. The displacement of individual strands cause nonuniform current sharing. Smith<sup>14)</sup> reports that in a 7 strand cable a negative current was observed in the central strand, when the field was pulsed with a few second rise time. All strands carried positive currents under d.c. conditions. Jüngst<sup>15)</sup> reports negative currents at low field levels even in not fully transposed cables.

Transposed cables, in which each strand occupies all positions within the cable cross-section, eliminate the above disadvantages but they have a low packing factor ( $\sim 40 - 50\%$ ) and a large number of cross over points. Strand breakage is observed, when a large number of them are used in the cable and compacted to specified cable sizes.

It was mentioned earlier that wire motion in the coil due to time variable Lorentz forces cause heat. The conduction of heat away from the superconductor to the bath may limit the coil current carrying capacity and generate conductor training. Two constructions to prevent wire motion are given below:

a) The cable is impregnated with In(Sn) or Ag(Sn) solder with an addition of Bi<sup>12)</sup>, or another eutectic. These impregnants have a relatively higher resistivity at 4.2K ( $>10^{-6}$  Ohm. cm) and coupling losses measured are only about a factor of two higher than in insulated cables.

b) Potting the cable in suitable thermosettings. In this case the individual strands are insulated with a layer of copperoxide or a thermosetting, compatible to the final potting mixture.

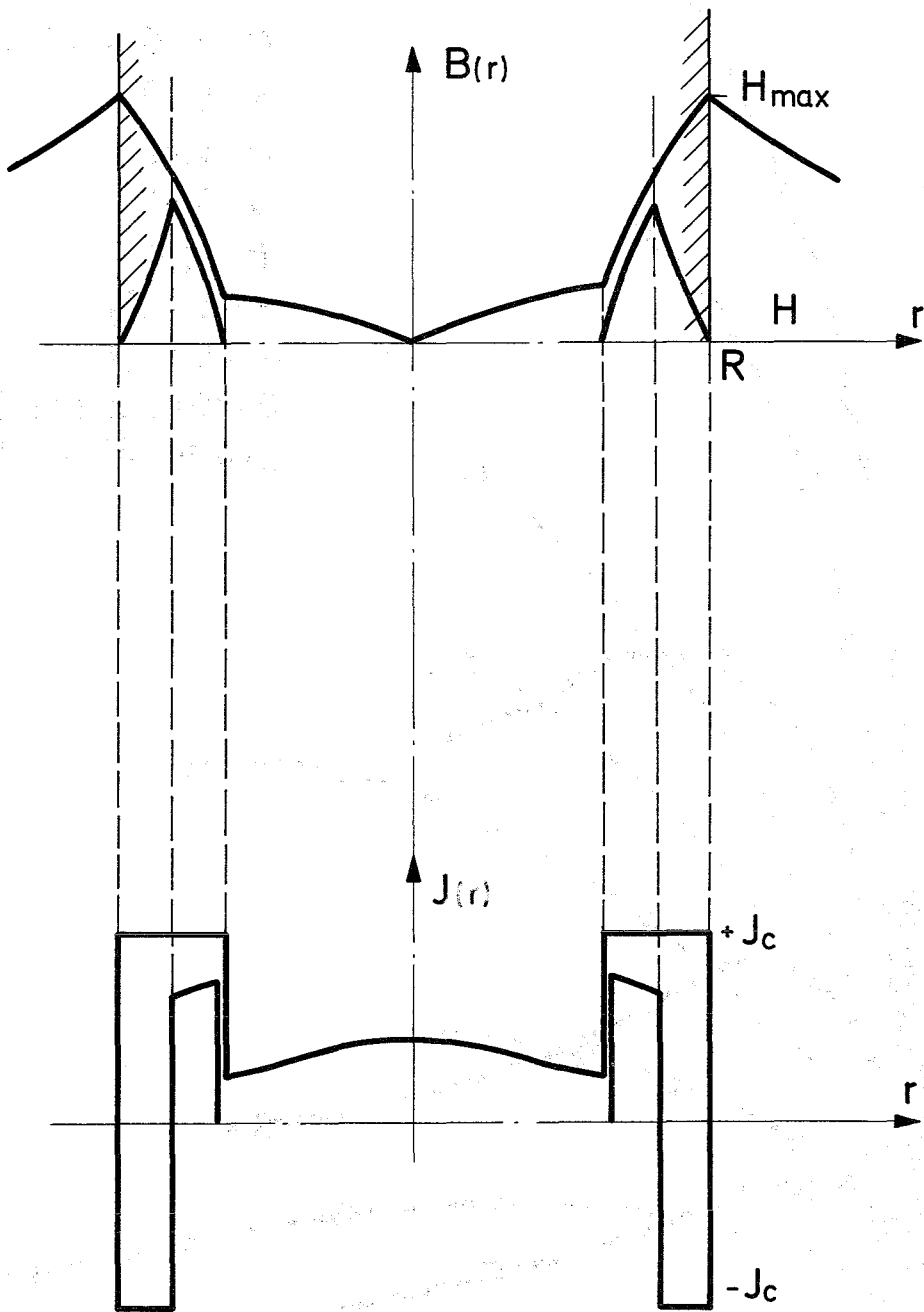


Fig. 2.3

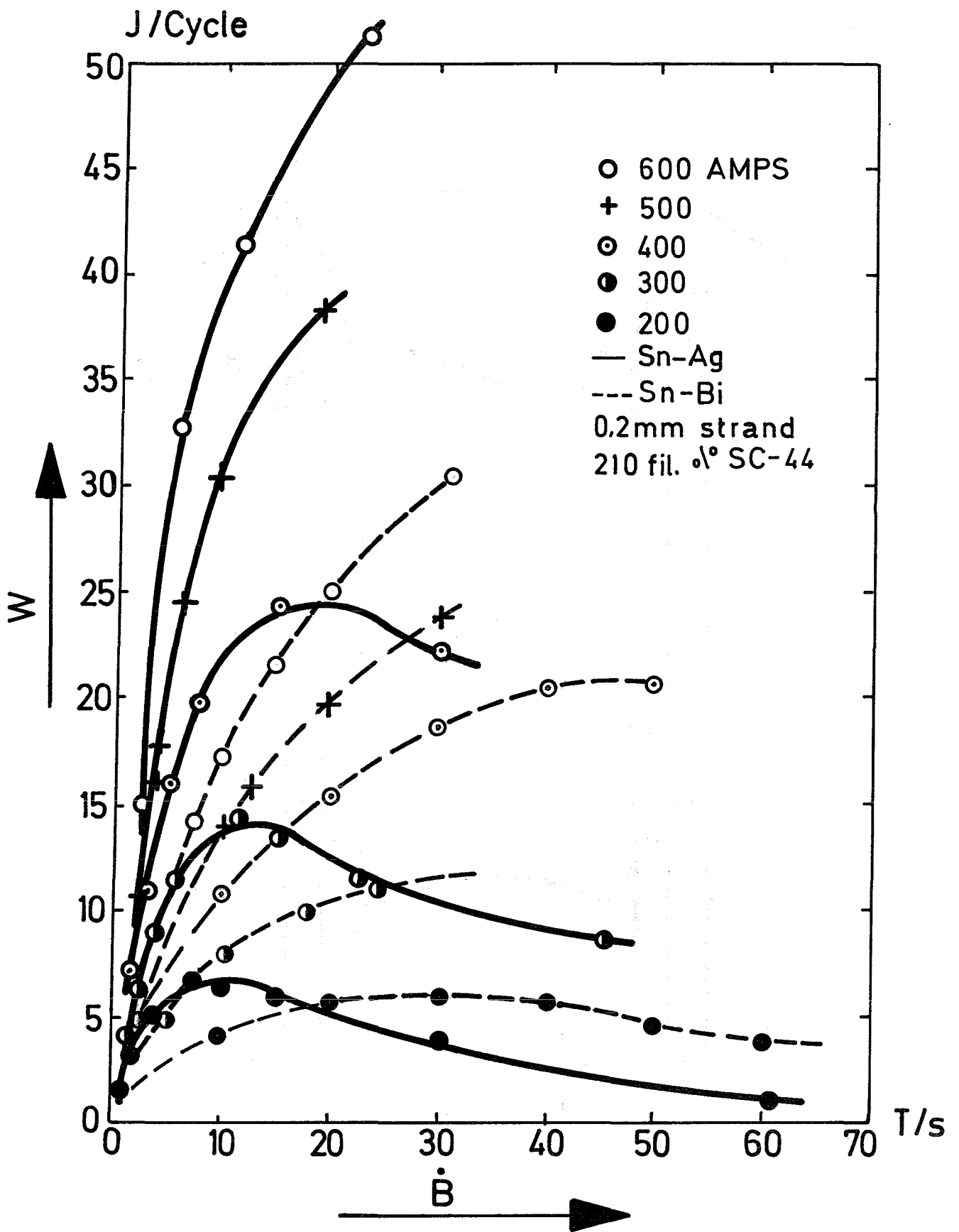


Fig.4.1

Fully insulated strands and cables, if potted, (type b) exhibit training after the first cool down. After each successive cool down training effects have been observed in some cases, in others no training effects have been observed, whence the coil was cooled repeatedly.<sup>14)</sup>

In soldered cables or braids (AgSn, or InSn) no training effects have been reported. Soldered cables have also the advantage of retaining their shape within the specified tolerances when bend over tight radii. This fact is important if reduced field tolerances within the useful aperture of the magnet are stringent. But even soldered conductors must be refrained from motion due to magnetomechanical forces, either by proper reinforcement, or potting in suitable epoxies, which have practically the same thermal contraction coefficient as the conductor and do not crack when cooled down thermally cycled and magnetically pulsed.

Metallic impregnated cables (type a) have operated better under pulsed conditions than not impregnated ones (type b). The reason may be found in the better heat transfer properties of the solder and the rigidity of the cable. One difficulty arising from the use of metallic insulated cables is the coupling between strands. This is the same phenomenon which causes also eddy current losses in the individual twisted strand. Additional eddy current losses occur in the cable depending from its twist rate. Induced eddy currents give an additional contribution to the irreversible sample magnetization which increases with  $\dot{B}$  and the twist length.

Fully insulated strands are totally decoupled. If the cable is coupled to any degree, say because of shorts between strands, or in metallic insulated cables due to the use of high resistivity solders, higher than about 20% of the total coupled case, cross-currents flowing through the high resistivity layers between strands generate losses far beyond the individual strand contribution and dominate the coil losses.

Fig. 4.1 gives the losses per cycle versus  $\dot{B}$  for solenoid using metallic insulated cables. It may be noted that losses per cycle are increasing with frequency in the low  $\dot{B}$  range and decreasing with frequency at high  $\dot{B}$  region as shown in Eq. (1.52), where

the factor  $1/|1+j\omega\tau|$  determines the shielding of  $\dot{B}$  in the interior of the conductor.

While theoretical predictions agree qualitatively with experimental results, quantitative agreement between measurement and theory is found in solenoid type coils. Measurements do agree with theory within a factor of two in race track shape coils (dipoles etc.). In tables 4.1, 4.2 and 4.3 losses measured in solenoids are compared to the theoretical predictions. No systematic measurements on a.c. losses were available on dipole magnets to enable a detailed comparison with theory.

Table 4.1

Comparison between calculated and measured a.c. losses  
in solenoids<sup>16)</sup>

Coil Geometry	$2a_1 = 6 \text{ cm}$ $2a_2 = 9 \text{ cm}$ $2b = 5.6 \text{ cm}$ $N = 2990$	$2a_1 = 2.4 \text{ cm}$ $2a_2 = 8.4 \text{ cm}$ $2b = 5.3 \text{ cm}$ $N = 5650$	$2a_1 = 2.4 \text{ cm}$ $2a_2 = 6.5 \text{ cm}$ $2b = 5.3 \text{ cm}$ $N = 6125$
Conductor	<u>IMI:</u> 61 fil. à 42 $\mu\text{m}$ $I_o H_o = 650 \text{ AT}$ $H_o = 1 \text{ T}$ $l = 705 \text{ m}$ $V_{\text{cond}} = 112 \text{ cm}^3$ $D = 0.045 \text{ cm}$	<u>AIRCO:</u> 361 fil. à 13 $\mu\text{m}$ $I_o H_o = 285 \text{ AT}$ $H_o = 1 \text{ T}$ $l = 958 \text{ m}$ $V_{\text{cond}} = 152 \text{ cm}^3$ $D = 0.045 \text{ cm}$	<u>VAC:</u> 61 fil. à 34 $\mu\text{m}$ $I_o H_o = 650 \text{ AT}$ $H_o = 1 \text{ T}$ $l = 856 \text{ m}$ $V_{\text{cond}} = 82.4 \text{ cm}^3$ $D = 0.033 \text{ cm}$
Matrix	<u>Cu:</u> $r = 180$ $\bar{\rho}_c = 4.7 \cdot 10^{-8} \text{ Ohm.cm}$ $l_{\text{pitch}} = 2.5 \text{ cm}$ $\tau = 21.10^{-3} \text{ s}$	<u>Cu:</u> $r = 70$ $\bar{\rho}_c = 7 \cdot 10^{-8} \text{ Ohm.cm}$ $l_{\text{pitch}} = 0.4 \text{ cm}$ $\tau = 1.45 \cdot 10^{-3} \text{ s}$	<u>Cu:</u> $r = 100$ $\bar{\rho}_c = 10 \cdot 10^{-8} \text{ Ohm.cm}$ $l_{\text{pitch}} = 0.6 \text{ cm}$ $\tau = 0.57 \cdot 10^{-3} \text{ s}$

$B_m(T)$	4.2				3.6					5.2			
Hysteretic losses (Ws/cycle) Eq.(1.28)	$W_{hl} = 9.23$ $\Delta I = 74 A$ $I_c = 325$ (at 1T)				$W_{hl} = 1.6$ $\Delta I = 36 A$ $I_c = 150 A$ (at 0.9T)					$W_{hl} = 10.3$ $\Delta I = 95 A$ $I_c = 370 A$ (at 1.25)			
Self field losses (Ws/cycle) Eq.(1.62)	$W_{sf} = 7.3 \cdot 10^{-3}$				$W_{sf} = 2.5 \cdot 10^{-3}$					$W_{sf} = 16.5 \cdot 10^{-3}$			
Field rise time $t_o/2$ (s)	5.6	8.77	15	25	2.5	4	5	6.5	10	1.8	3.6	6.25	10
Eddy Current losses (Ws/cycle)Eq.(1.52)	8.44	5.06	3.0	1.78	1.2	0.76	0.61	0.5	0.3	0.752	0.38	0.22	0.135
Total calculated losses (Ws/cycle)	17.7	14.31	12.25	11.03	2.8	2.36	2.21	2.1	1.9	11.5	10.7	10.52	10.44
Total measured losses (Ws/cycle)	21	15.8	10.8	10.0	3.75	2.16	1.5	1.25	1.2	10.5	10.1	10	10

Table 4.2

Comparison between calculated and measured a.c. losses  
in solenoids<sup>17)</sup>

Coil Geometry	$2a_1 = 5 \text{ cm}$ $2a_2 = 9 \text{ cm}$ $2b = 7.5 \text{ cm}$ $N = 4000$	$2a_1 = 5 \text{ cm}$ $2a_2 = 9 \text{ cm}$ $2b = 7.5 \text{ cm}$ $N = 4000$	$2a_1 = 5 \text{ cm}$ $2a_2 = 9 \text{ cm}$ $2b = 7.5 \text{ cm}$ $N = 4000$
Conductor:	<u>VAC:</u> 61 fil. à 34 $\mu\text{m}$ $I_0 H_0 = 840 \text{ AT}$ $H_0 = 1 \text{ T}$ $l = 780 \text{ m}$ $V_{\text{cond}} = 67 \text{ cm}^3$ $D = 0.033 \text{ cm}$	<u>VAC:</u> 61 fil. à 34 $\mu\text{m}$ $I_0 H_0 = 840 \text{ AT}$ $H_0 = 1 \text{ T}$ $l = 780 \text{ m}$ $V_{\text{cond}} = 67 \text{ cm}^3$ $D = 0.033 \text{ cm}$	<u>VAC:</u> 61 fil. à 34 $\mu\text{m}$ $I_0 H_0 = 840 \text{ AT}$ $H_0 = 1 \text{ T}$ $l = 780 \text{ m}$ $V_{\text{cond}} = 67 \text{ cm}^3$ $D = 0.033 \text{ cm}$
Matrix:	<u>Cu:</u> $r = 100$ $\bar{\rho}_c = 10 \cdot 10^{-8} \text{ Ohm.cm}$ $l_{\text{pitch}} = 0.2 \text{ cm}$ $\tau = 0.07 \cdot 10^{-3} \text{ s}$	<u>Cu:</u> $r = 100$ $\bar{\rho}_c = 10 \cdot 10^{-8} \text{ Ohm.cm}$ $l_{\text{pitch}} = 0.3 \text{ cm}$ $\tau = 0.14 \cdot 10^{-3} \text{ s}$	<u>Cu:</u> $r = 100$ $\bar{\rho}_c = 10 \cdot 10^{-8} \text{ Ohm.cm}$ $l_{\text{pitch}} = 0.6 \text{ cm}$ $\tau = 0.57 \cdot 10^{-3} \text{ s}$

$B_m(T)$	4				4				4			
Hysteretic losses (Ws/cycle) Eq.(1.28)	$W_{hl} = 9.5$				$W_{hl} = 9.5$				$W_{hl} = 9.5$			
Self field losses (Ws/cycle) Eq.(1.62)	$10^{-2}$				$10^{-2}$				$10^{-2}$			
Field rise time $t_o/2$ (s)	1	2	5	10	0.5	1	2	5	0.5	1	2	5
Eddy current losses (Ws/cycle) Eq.(1.52)	$70 \times 10^{-3}$	$35 \times 10^{-3}$	$14 \times 10^{-3}$	$7 \times 10^{-3}$	0.32	0.16	0.08	0.032	1.28	0.64	0.32	0.13
Total calculated losses (Ws/cycle)	9.57	9.53	9.51	9.5	9.82	9.66	9.58	9.53	10.78	10.14	9.82	9.63
Total measured losses (Ws/cycle)	9.8	9.8	9.8	9.8	13.2	11.8	10.9	10.1	13.8	12.2	10.7	9.0

Table 4.3

Comparison between calculated and measured a.c. losses  
in solenoids<sup>16)</sup>

Coil Geometry	<u>I</u>	<u>II</u>	<u>III</u>
Conductor	<u>IMI</u> : 61 fil. à 28 μm $I_0 H_0 = 300 \text{ AT}$ $H_0 = 1 \text{ T}$ $l = 563 \text{ m}$ $V_{\text{cond}} = 39.5 \text{ cm}^3$ $D = 0.03 \text{ cm}$	<u>IMI</u> : 61 fil. à 28 μm $I_0 H_0 = 300 \text{ AT}$ $H_0 = 1 \text{ T}$ $l = 223 \text{ m}$ $V_{\text{cond}} = 15.6 \text{ cm}^3$ $D = 0.03 \text{ cm}$	<u>Supercon</u> 16x400 fil. à 7.5 μm $I_0 H_0 = 1400 \text{ AT}$ $H_0 = 0.7 \text{ T}$ $l = 296 \text{ m}$ $V_{\text{cond}} = 150 \text{ cm}^3$ 16 strand transposed cable
Matrix	<u>Cu</u> : $r = 180$ $\bar{\rho}_c = 4.7 \cdot 10^{-8} \text{ Ohm.cm}$ $l_{\text{pitch}} = 0.25 \text{ cm}$ $\tau = 0.2 \cdot 10^{-3} \text{ s}$	<u>Cu</u> : $r = 180$ $\bar{\rho}_c = 4.7 \cdot 10^{-8} \text{ Ohm.cm}$ $l_{\text{pitch}} = 0.25 \text{ cm}$ $\tau = 0.2 \cdot 10^{-3} \text{ s}$	<u>Cu</u> : $r = 100$ $\bar{\rho}_c = 7 \cdot 10^{-8} \text{ Ohm.cm}$ $l_{\text{pitch}} = 0.2 \text{ cm}$ $\tau = 0.2 \cdot 10^{-3} \text{ s}$

$B_m$ (T)	1	2	3	4	1	2	3	1	2	3	4
Hysteretic losses (Ws/cycle) Eq.(1.28)	0.81	1.38	1.83	2.2	0.32	0.5	0.7	0.69	1.15	1.5	1.76
Field rise time $t_o/2$ (s)		2			2			2			
$B_m$ (T)		4			3			3			
Eddy current losses (Ws/cycle) Eq.(1.52)	No frequency dependence obs. $W_e = 0.07$				No Frequency dependence obs. $W_e = 0.016$			No Frequency dependence obs. 0.007 0.029 0.064 0.114			
$B_m$ (T)		4			4			4			
Self field losses (Ws/cycle) Eq.(1.62)	$\Delta I = 57A$ $I_c = 150$ (at 1T) $W_{sf} = 6 \times 10^{-3}$				$\Delta I = 59A$ $I_c = 170A$ (at 0.75) $W_{sf} = 2.2 \cdot 10^{-3}$			$\Delta I = 12A/\text{strand}$ $I_c = 51A$ (at 1T) $W_{sf} = 1.35 \cdot 10^{-3}$			
Total calculated losses (Ws/cycle)	0.886	1.456	1.906	2.27	0.338	0.568	0.75	0.7	1.118	1.56	1.88
Total measured losses (Ws/cycle)	0.58	1.1	1.5	1.85	0.27	0.5	0.7	0.73	1.26		

## 5. Methods of Loss measurement

Methods to measure a.c. losses in superconductors can be implied to test samples and specimen and to measure losses in coils. Popular methods to measure losses are the calorimetric method, in which the additional helium boil off due to a.c. losses is measured and the electric method at which instantaneous values of the current and voltage are multiplied and integrated over the time.

### 5.1 Calorimetric method:

Fig. 5.1 illustrates the method of loss measurement of specimen schematically. The specimen is wound bifilar and placed in a calorimeter. The superconductor is energized from a pulse-generator, or a variable current, low frequency ( $\leq 50$  Hz) source. The helium boil-off due to a.c. losses is measured by means of a gas flowmeter. The calorimeter is placed in a main liquid helium dewar, such that current leads are located inside the main cryostat prior to entering the calorimeter.

The sensitivity of the method ( $\sim 1$  mW) is moderate, if low frequency pulsing is applied. The measurement accuracy is improved by increasing pulse frequency. The advantage of this method is its independence on magnetic energy stored in the coil. Its main disadvantage, the long time required until equilibrium conditions are established to measure losses. Only magnets of moderate size have been tested with this method.

### 5.2 Electric methods:

Several methods are used successfully and in the following a description of few methods is given. The basic principle of this method is to generate a voltage which is proportional to the power delivered to the coil and integrating it over one or several cycles.

The circuit shown in Fig. 5.2 is described by Gilbert<sup>19)</sup> and is used to measure a.c. losses in superconducting samples and coils. The circuit consists to two major parts:

A multiplying circuit to obtain instantaneous power flow between specimen (coil) and a powersupply and an integrator to keep track of the energy delivered into the superconducting magnet.

The multiplying circuit operates as follows: It utilizes a Hall-probe which generates an output voltage proportional to the product of input current to the Hallprobe and the magnetic field around the probe. The test magnet is connected to the Hallprobe through a resistor by a pair of potential leads inserted into the cryostat. Thus the input current to the Hallprobe is proportional to the magnet voltage. The Halldevice is mounted in the gap of a coil which generates a magnetic field proportional to the transport current of the coil, ( $B_s = K.I.$ ). As this coil is connected in series to the superconducting magnet to be tested, the Halldevice is exposed to a magnetic field proportional to the current flowing through the superconducting magnet. The input to the Halldevice is thus proportional to the voltage accross the superconducting magnet and to the magnet current. The output voltage of the Halldevice is proportional to the instantaneous value of the power into the superconducting magnet.

The integrator uses a solid state chopper operational amplifier with a feed back capacitor C and a series resistor R, such that its output voltage is 
$$U_{out} = \frac{1}{RC} \int_0^T U_{in}(t) dt.$$

The drift in the integrator circuit appears as an equivalent power loss and must be kept small. (1mV-drift in  $10^3$  sec, with a dynamic range of 10V).

The Hall voltage is integrated by means of an integrator. The output voltage is given by:

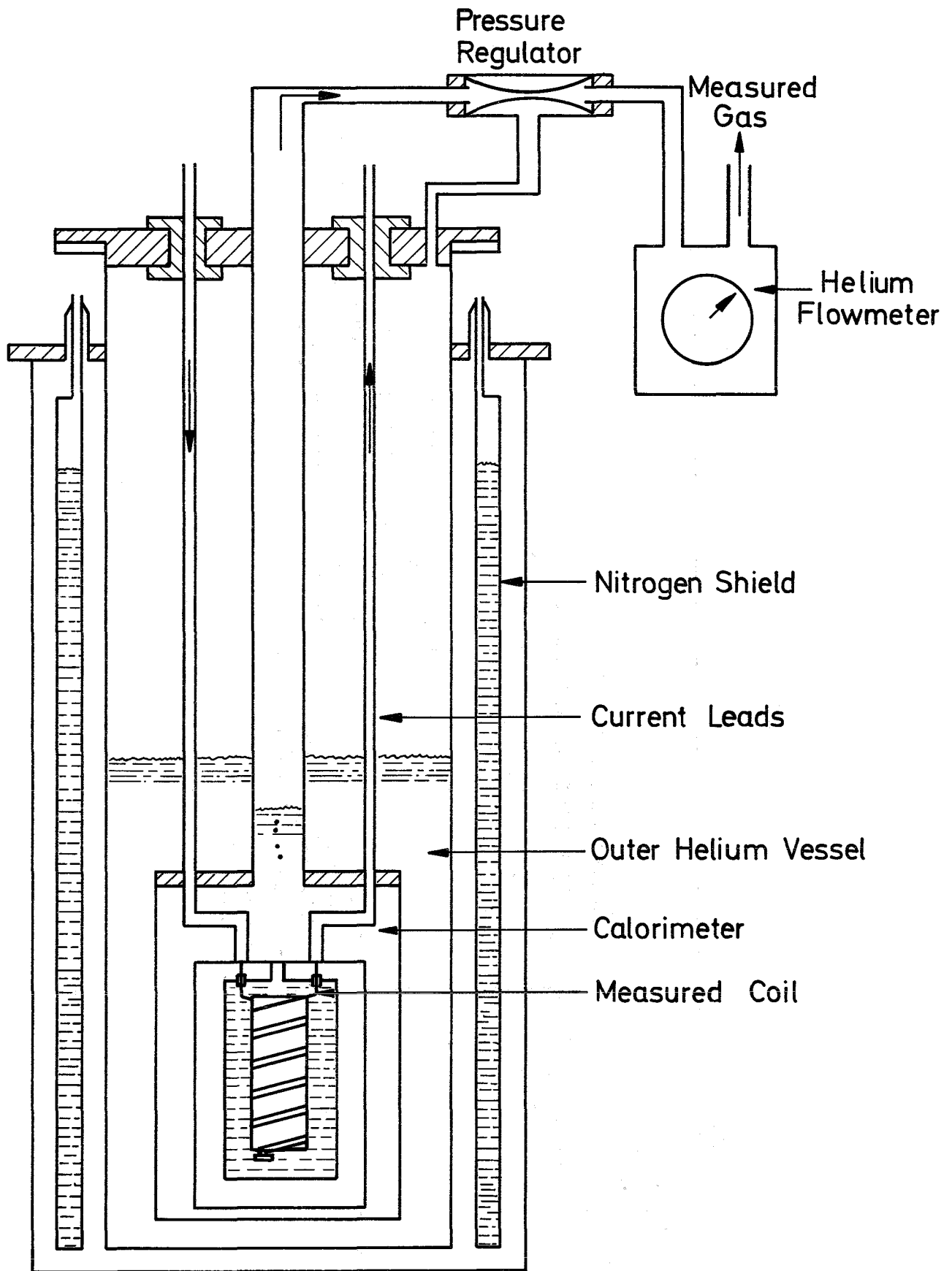


Fig. 5.1

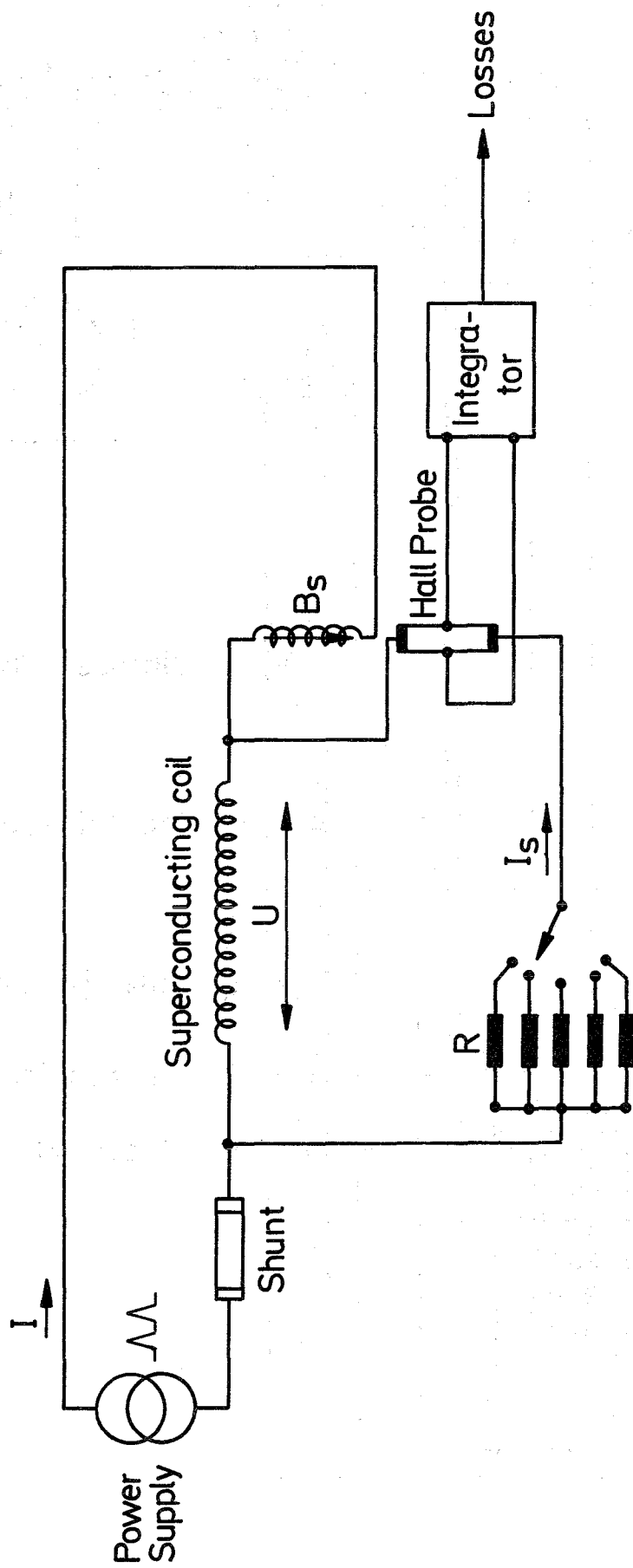


Fig. 5.2

$$U_0 = \frac{s \cdot K}{\tau \cdot R} \cdot W \leq \frac{s \cdot B_{s,max} \cdot I_s}{\tau \cdot I_{max} \cdot U_{max}} \cdot W \quad (5.1)$$

where  $W$  are the losses to be measured,  $s$  is the sensitivity and  $I_s$  the maximum current through the Hallprobe;  $B_{x,max}$  is the maximum fluxdensity determined by the nonlinearity of the Hallprobe.  $\tau$  is the time constant of the feed-back loop of the integrator and  $U_{max}$ ,  $I_{max}$  the maximum voltage and maximum current resp., applied to the superconducting coil during the cycle.

It is seen from the above relation, that the sensitivity of the method is limited by the characteristics of the Hallprobe ( $s$ ,  $I_s$ ,  $B_{s,max}$ ) and by the magnitude of the applied voltage and current. The circuit has a moderate sensitivity of about  $\pm 5\%$  at  $Q \leq 100$ ,

The sensitivity of the system is also limited by the drift of the integrator, its nonlinearity and by the thermoelectric voltage of the Hallprobe.

To reduce the influence of the inductive term  $U_{max}$ , Hlasnik<sup>20)</sup> and coworker have proposed its compensation by means of a linear mutual inductance, whose primary side is in series to the superconducting coil and whose secondary side compensates the inductive component of the coil voltage, as shown in Fig. 5.3. The voltage  $U_d$  is essentially resistive component and can be amplified and applied to the Hallprobe. The sensitivity of this method is about a factor of 20 better than in the previous scheme. The circuit is more susceptible for measuring losses in coil using multifilament composite conductors.

The circuit proposed by Fietz<sup>21)</sup> is useful to obtain hysteretic losses in specimen. The sample is inserted into the gap of one of the two coils of identical cross sectional area and identical number of turns placed side by side in the solenoid generating the external field. (Fig. 5.4)

As long as the sample is not superconducting, the output induced voltage from the coils 2 and 3 are the same and cancel each other in the circuit. A coarse and a fine potentiometer correct for small voltage deviations due to measuring coil errors.

The measuring coil 2 and 3 are designed to fit the specimen closely such that a good inductive coupling between sample and coil is obtained. The difference voltage from the coils (empty coil and coil with specimen) is amplified by an operational amplifier. The integrated voltage  $U_0$  is proportional to the magnetization of the specimen. Tracing this voltage against the integrated induced voltage in a pick up coil (proportional to the external field) a magnetization curve such shown in Fig. 5.5 for NbTi is obtained. The area of the magnetization curve is proportional to the hysteretic losses for one cycle.

Error sources are due to deviations in the area or number of turns of the measuring coils, the positioning of these coils in the external field, unmatched flux densities (different Ampereturns in the coils) and mainly errors due to the drift of the operational amplifier. The circuit has been also used by McInturff<sup>22)</sup> to measure magnetization losses of NbTi wires.

An apparatus to measure low frequency losses is described by Sekula<sup>23)</sup>.

Another electric method to measure losses is given by Pech<sup>24)</sup>.

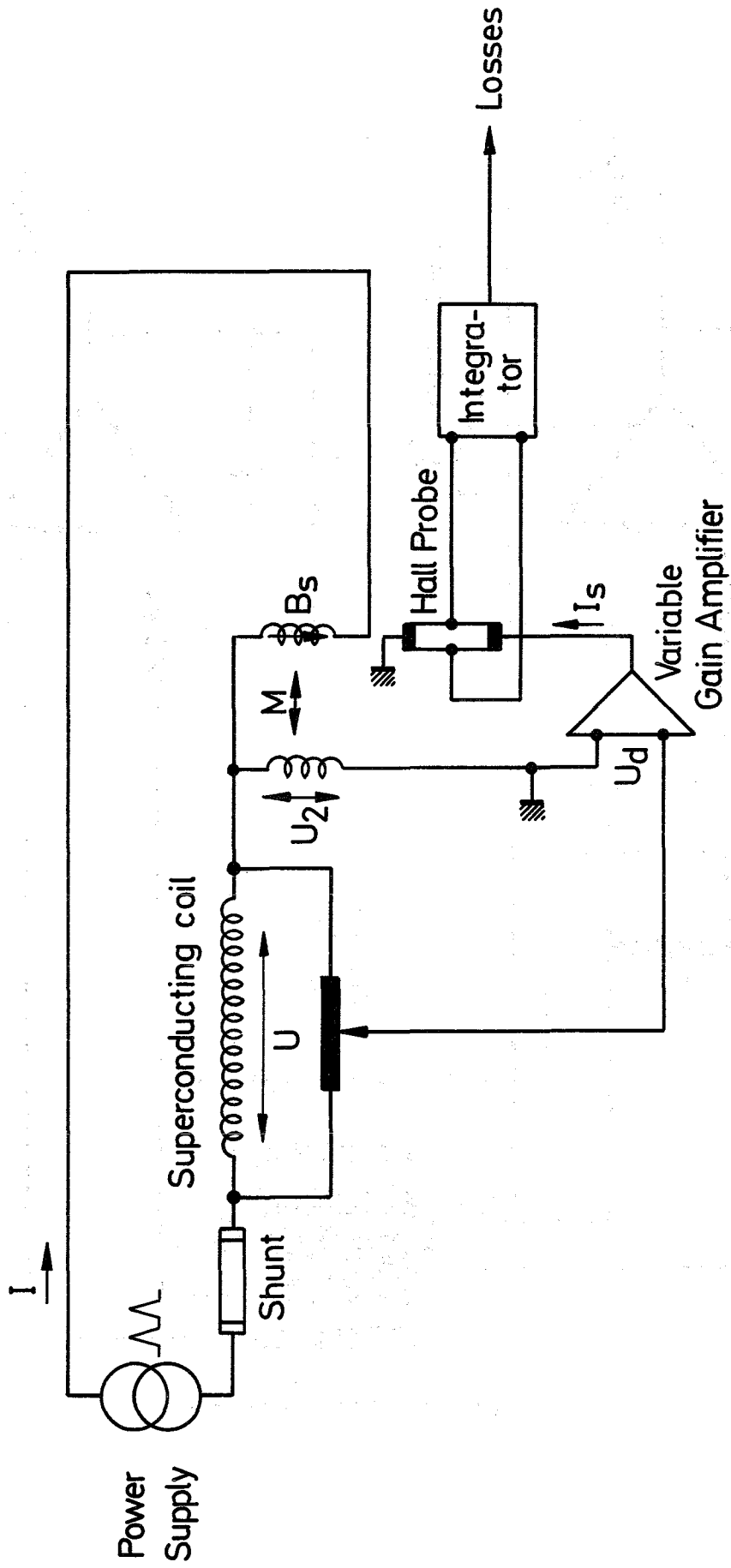


Fig. 5.3

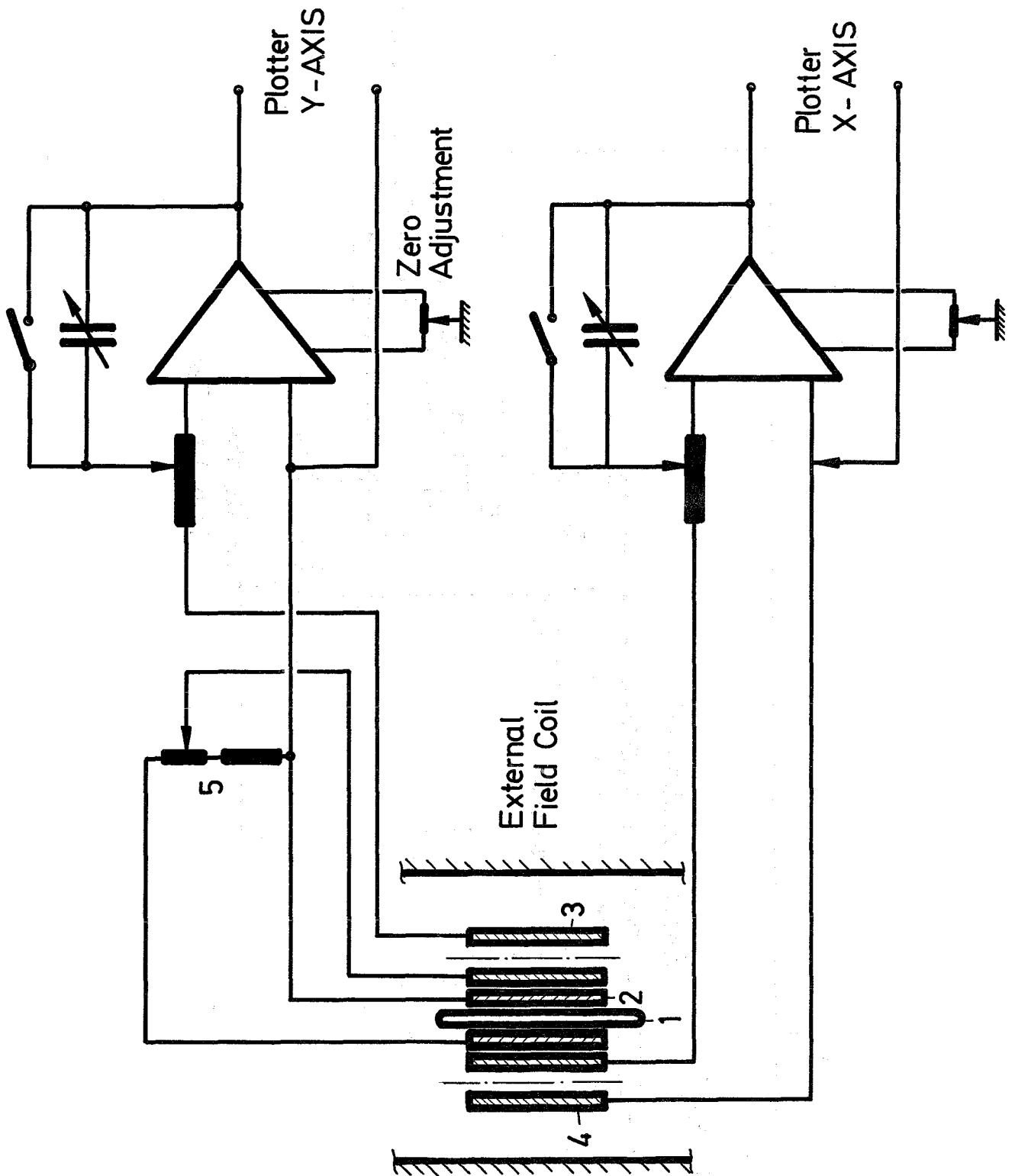


Fig. 54

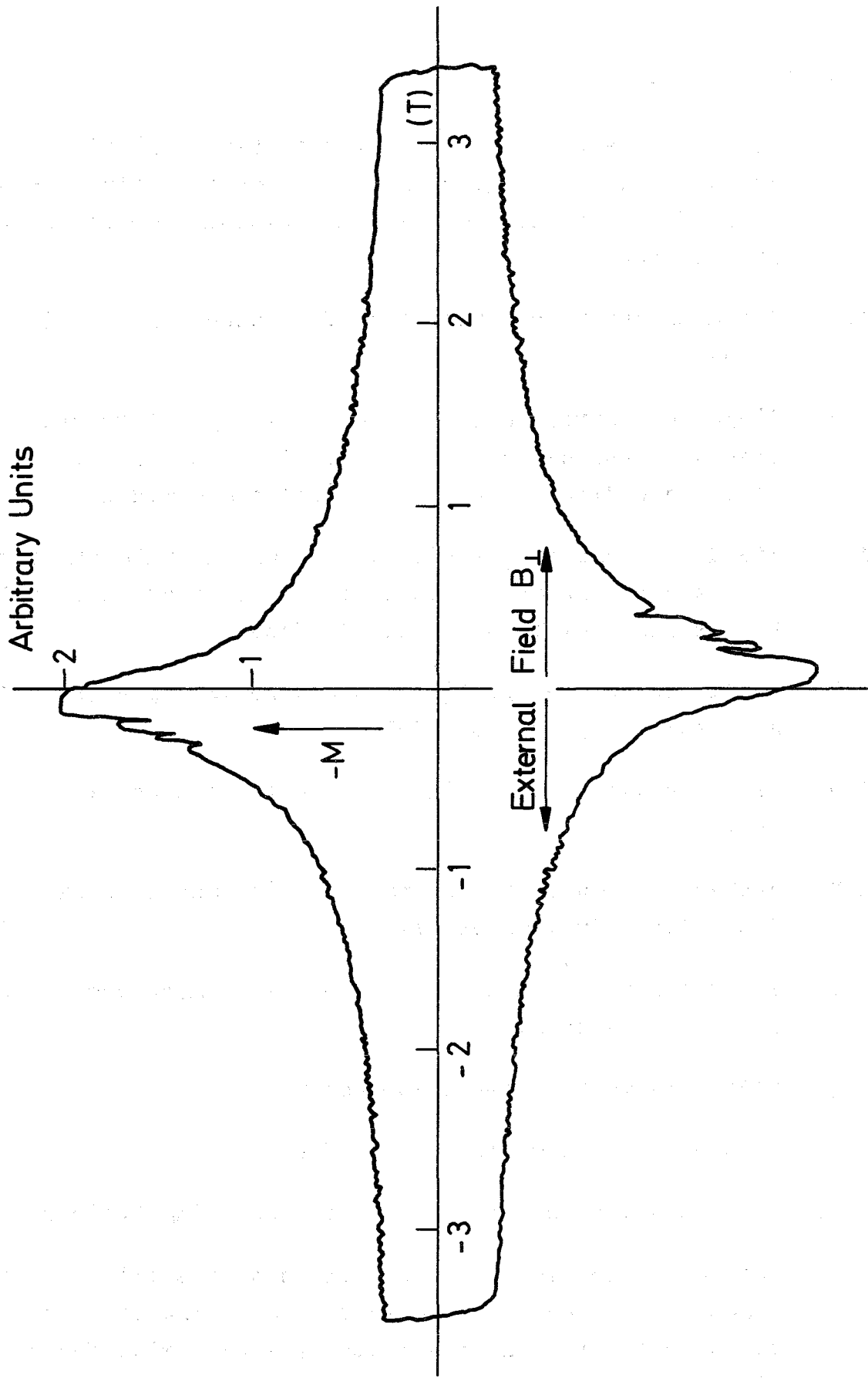


Fig. 5.5

Figure Captions:

- 1.1 Schematic representation of the spatial variation of free energy of a flux line or a bundle of flux lines in a real type II superconductor with and without impressed transport currents.
- 1.2 Field penetration into a type II superconductor with pinning.
- 1.3 Field and current distribution in a type II superconducting slab with the external field parallel to the surface of the slab, according to Bean's critical state model.
- 1.4 Field and current distribution in an infinite sheet due to the application of transport currents and external fields parallel to the sheet surface.
- 1.5 Field and current profiles in a type II superconducting slab according to Kim Model.
- 1.6 Field penetration profile in a semi-infinite slab (Kim Model).
- 1.7 Hysteretic losses vs. characteristic conductor parameters  $J_0 B_0 d$  for a 1m long dipole.
- 1.8 Schematic representation of a multifilament conductor with twisted filaments.
- 1.9 Composite multifilament conductor.
- 1.10 Pulsed fields and induced currents.
- 1.11 Field profile in a type II superconducting cylinder.
- 1.12 Energy dissipation per unit length of specimen vs. peak transport current.<sup>10)</sup> The loss at the critical current for each specimen is indicated by a triangle. The dashed line is according to Hancox<sup>9)</sup> expression.

- 1.13 Comparison between self field and hysteric losses for a pulsed magnet with 5T peak field at  $5 \times 10^4$  A/cm<sup>2</sup> overall current density and vs. Composite.
- 2.1 Composite conductor with twisted superconducting filaments.
- 2.2 Axial diffusion of transport currents through a normal joint into a composite conductor.  
top: Current path.  
bottom: Current distribution.
- 2.3 Self field and current density pattern in a cylindrical conductor.
- 4.1 Energy dissipation vs.  $\dot{B}$ . A flat fully transposed braid used in the solenoid with Id = 2.5 cm; OD = 7.6 cm; length = 4.75 cm has 33 strands with 210 filaments each. Each strand has a diameter of 0.02 cm and the filaments have a diameter of  $\sim 12$  m typically. The matrix is copper.<sup>8)</sup>
- 5.1 Schematic representation of the calorimetric method to measure a.c. losses.
- 5.2 Schematic arrangement of a.c. loss-measuring electrical method.
- 5.3 Electrical a.c. loss-measuring method using an inductive compensating coil.
- 5.4 Circuit diagram according Fietz<sup>21)</sup>.
  1. Sample
  2. Sample coil
  3. Bucking coil
  4. Field measuring coil
  5. Fine and crude potentiometers
- 5.5 Typical hysteresis curve measured for NbTi.

## References:

1. Labusch, R., Crystal Lattice Defects 1, 1, (1969)
2. Beasley, M.R., Labusch, R., and Webb, W.W. Phys.Rev. 43  
682 (1969)
3. Friedel, I., De Gennes, P.G., and Matricon, J., Appl. Phys.  
Lett. 2, 119 (1963)
4. Bean, E.P., Rev. Mod. Phys. 36, 31 (1964)
5. Kim, Y.B., Hempstead, C.F., and Strnad, A.R., Phys. Rev. 131,  
6, 2486 (1963)
6. Morgan, G.H. BNL int.rep. AA DD-146 (1968)
7. Morgan, G.H., J. Appl. Phys. 41 3673 (1970)
8. Mc Inturff A.D. et.al. BNL int.rep. AA DD-179 (1971)
9. Hancox, R., Proc. IEE 113, 1221 (1966)
10. Salmon, D.R., and Catterall, I.A., J.Phys. D: Appl. Phys. 3,  
1023 (1970)
11. Pouillange, I.P., and Prost, G., GATS/71-24 (1971)
12. Spurway, A.H., Lewin, I.D., Smith P.F., J.Phys. D:  
Appl. Phys. 3, 1517 (1970)
13. Bronca, G., et.al. Proc. 3d. Intnatl. Conf. on Magnet  
Tech. Hamburg (1970)
14. Smith, P.F., Proc. 8th Intnatl. Conf. on High Energy  
Acc. CERN, 35 (1971)
15. Jüngst, K.P. Private Com.
16. Jüngst, K.P., Krafft, G., and Ries, G., KFK 1217 (1970)
17. Bogner, G., Salzburger, H., and Franksen, H., Proc. 3d  
Intnatl. Conf. Magnet. Tech. Hamburg (1970)
18. Bronca, G. et.al., GATS/70-37 (1970)
19. Gilbert, W.S., Hintz, R.E., Voelker, F., U.CRL-18176 (1968)
20. Hlasnik, G., Lefrancois, I.P., and Pouillange, I.P.,  
SEDAP 69-308-Sup. 84 (1969, and SEDAP 18/11 (1969)
21. Fietz, W.A. The Rev. Sci Instr. 36, 11 1621 (1965)
22. Mc Inturff, A.D., Proc. 1968 BNL Summer Study part II, 465  
(1968), BNL 50155 (C-55)
23. Sekula, S.T., J.Appl. Phys. 42, 1, 16 (1971)
24. Pech, T., Rev. Phys. Appl. Tome 5, 357 (1970)